AD-A076 504　　NEW JERSEY INST OF TECH　NEWARK　　　　　　　　F/G 20/14
RADIATION FROM INTEGRATED DIELECTRIC MILLIMETER-WAVE SLAB-WEDGE--ETC(U)
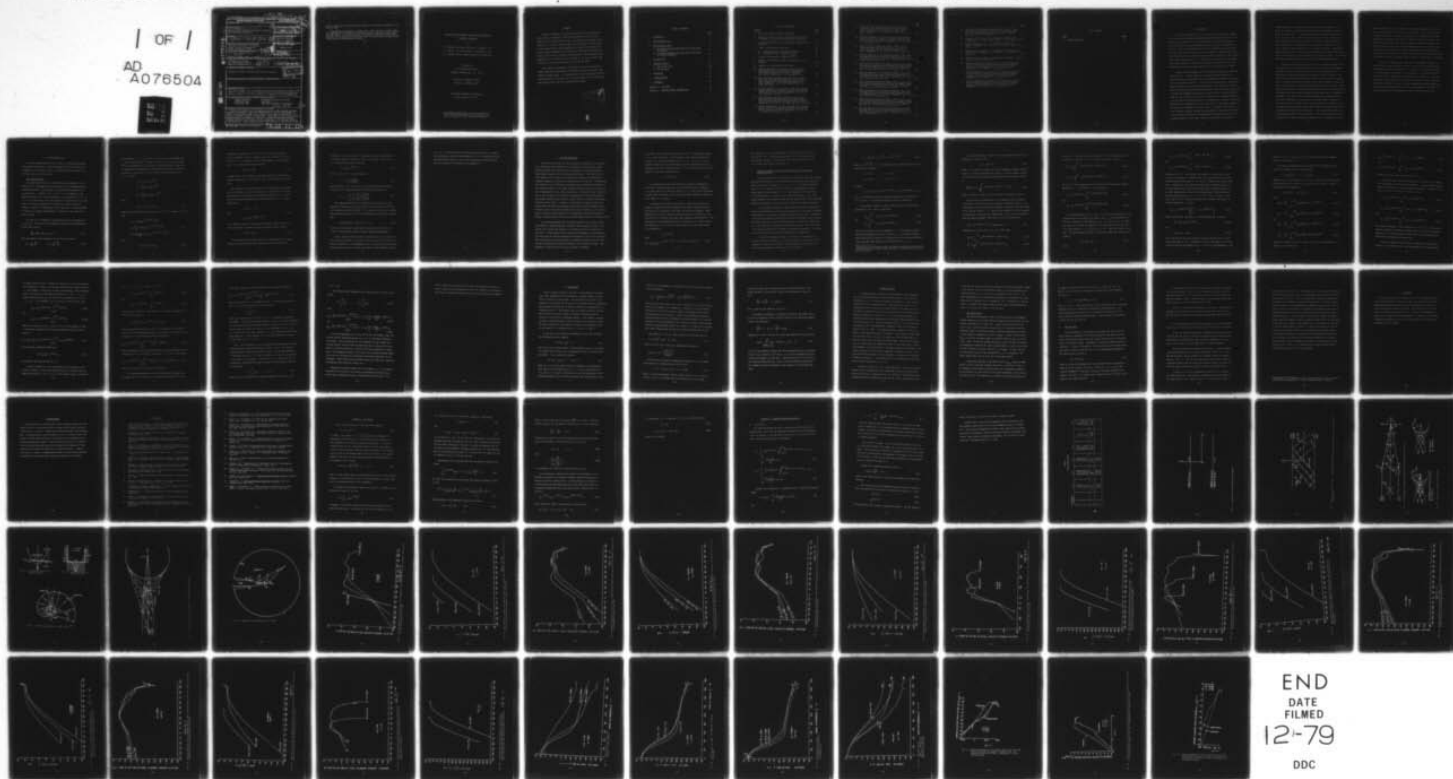OCT 79　G M WHITMAN , S J MAURER , A R NOERPEL　DAAG29-76-G-0131
UNCLASSIFIED　　　　　　　　　　　　　　ARO-13677.2-ELX　　　　　　　NL

| OF |
AD
A076504

END
DATE
FILMED
12-79
DDC

SECURITY CLASSIFICATION OF THIS PAGE *(When Data Entered)*

18 ARO 13677. 2-ELX

REPORT DOCUMENTATION PAGE

READ INSTRUCTIONS
BEFORE COMPLETING FORM

1. REPORT NUMBER	2. GOVT ACCESSION NO.	3. RECIPIENT'S CATALOG NUMBER

4. TITLE *(and Subtitle)*	5. TYPE OF REPORT & PERIOD COVERED
Radiation from Integrated Dielectric Millimeter-Wave Slab-Wedge Structures	Final Technical Report 29 Jan 1976— 31 May 1979
	6. PERFORMING ORG. REPORT NUMBER

7. AUTHOR(s)	8. CONTRACT OR GRANT NUMBER(s)
G. M. Whitman, S. J. Maurer, A. R. Noerpel	DAAG29-76-G-0131 DAAG29-77-G-0094

9. PERFORMING ORGANIZATION NAME AND ADDRESS	10. PROGRAM ELEMENT, PROJECT, TASK AREA & WORK UNIT NUMBERS
New Jersey Institute of Technology Newark College of Engineering Newark, New Jersey 07102	DRXRD-EL-13677

11. CONTROLLING OFFICE NAME AND ADDRESS	12. REPORT DATE
U. S. Army Research Office P. O. Box 12211 Research Triangle Park, NC 27709	October 1979
	13. NUMBER OF PAGES 72

14. MONITORING AGENCY NAME & ADDRESS *(if different from Controlling Office)*	15. SECURITY CLASS. *(of this report)*
Department of the Army U.S. Army Research Office Research Triangle Park, N. C. 27709	Unclassified
	15a. DECLASSIFICATION/DOWNGRADING SCHEDULE

16. DISTRIBUTION STATEMENT *(of this Report)*

Approved for public release; distribution unlimited.

RECEIVED NOV 14 1979

17. DISTRIBUTION STATEMENT *(of the abstract entered in Block 20, if different from Report)*

18. SUPPLEMENTARY NOTES

19. KEY WORDS *(Continue on reverse side if necessary and identify by block number)*

Tapered dielectric	Integrated dielectric structure
Dielectric wedge	Ray optics
Dielectric slab	Plane Wave integral representation

392 024

20. ABSTRACT *(Continue on reverse side if necessary and identify by block number)*

A method of analysis of an integrated dielectric slab waveguide and wedge radiator is presented. Plane wave constituents in the slab are assumed to excite the dielectric wedge. The solution in the wedge is postulated to be a finite, continuous spectrum of plane waves. Reflections of these waves from the wedge boundaries are taken into account by introducing angularly dependent Fresnel reflection coefficients into the integrands of the planewave integral representations. These integrals reduce asymptotically to the dielectric slab

DD FORM 1 JAN 73 1473 EDITION OF 1 NOV 65 IS OBSOLETE

SECURITY CLASSIFICATION OF THIS PAGE *(When Data Entered)*

fields in the limit of small wedge apex angle at the interface between the slab and the wedge.

Using numerical techniques, the TE surface fields and the far field radiation patterns are determined for different dielectric materials, wedge lengths and slab widths. It is observed that by decreasing either the relative permittivity of the dielectric or the slab width or by increasing the wedge length a more directive antenna pattern results.

RADIATION FROM INTEGRATED DIELECTRIC MILLIMETER-WAVE

SLAB-WEDGE STRUCTURES

by

G. M. Whitman, New Jersey Institute of Technology, N.J.

S. J. Maurer, New York Institute of Technology, N.Y.

A. R. Noerpel, Bell Telephone Laboratories, Holmdel,N.J.

Prepared for

U.S. Army Research Office

Research Triangle Park, N.C. 27709

Contract No. DAAG29-77-G-0094

Project No. DRXRO-EL-13677

New Jersey Institute of Technology

Newark, New Jersey 07102

ABSTRACT

A method of analysis of an integrated dielectric slab waveguide and wedge radiator is presented. Plane wave constituents in the slab are assumed to excite the dielectric wedge. The solution in the wedge is postulated to be a finite, continuous spectrum of plane waves. Reflections of these waves from the wedge boundaries are taken into account by introducing angularly dependent Fresnel reflection coefficients into the integrands of the plane wave integral representations. These integrals reduce asymptotically to the dielectric slab fields in the limit of small wedge apex angle at the interface between the slab and the wedge.

Using numerical techniques, the TE surface fields and the field radiation patterns are determined for different dielectric materials, wedge lengths and slab widths. It is observed that by decreasing either the relative permittivity of the dielectric or the slab width or by increasing the wedge length a more directive antenna pattern results.

-i-

TABLE OF CONTENTS

LIST OF ILLUSTRATIONS

LIST OF TABLES

1. INTRODUCTION

The current availability of low loss silicon has provided the capabil-
ity of constructing miniature integrated waveguide and antenna devices. Such
devices are of interest to U.S. Army scientists for use in the millimeter
wave transmitters and receivers being developed to improve data transmission
rates [1]. Since the antenna structures under consideration are constructed
from dielectric materials (silicon), they are tapered to improve their radia-
tion characteristics (increased pattern directivity and lower side lobe levels)
over a wide frequency band [1-4]. Although rigorous theoretical approaches to
study tapered dielectric structures in principle are available [12,13], the
solution to the dielectric wedge problem has not been worked out in detail.

Tapered dielectric geometries have been analyzed using local mode type
theories [6-11]. In these theories, the guided wave characteristics of a
tapered structure are determined from the corresponding waveguide characteris-
tics of the untapered structure. A first order solution based on Shevchenko's
rigorous approach [12] yields local mode results. Both Marcuse [8,9] and, to
first order, Shevchenko [12] obtained approximate solutions for the field along
a tapered slab waveguide joining two dielectric slabs of different heights in
terms of a local surface wave by using a complete set of transverse mode func-
tions and presented different methods for determining the expansion coefficients.
Balling [6,7,14] examined the near and far fields of a line source imbedded in
an infinite two-dimensional dielectric wedge. He compared a WKB solution to
a more accurate one based on plane wave superposition integrals which allowed
for ray optical and lateral ray interpretations. Methods using ray optics to
determine asymptotic (ray) modal fields in non-radiating, non-uniform or

-1-

tapered geometries (with boundary conditions which allow solutions to be obtained by separation of variable techniques) have been thoroughly studied by Maurer and Felsen [15-18]. Their approach, however, does not apply directly to the dielectric wedge. Bates [5] confirmed the conclusion of Maurer and Felsen that source-free modal solutions for dielectric wedge structures cannot be constructed. The rigorous, Full Wave approach of Bahar [13] can be used to study the wedge problem, but it is extremely difficult. Shevchenko's rigorous approach [12], which is similar to Bahar's, would require higher order terms to be applicable to the wedge problem. An excellent survey of work done on the dielectric wedge problem can be found in Balling's dissertation [6].

The method of analysis presented here, which provides meaningful physical insight into the wave processes taking place in a dielectric slab-wedge integrated structure, is based on the work of Maurer and Siwiak [19,20]. In that theory, a finite wedge segment is excited by a single slab mode. The field in the dielectric wedge region is inferred from an integral representation of a Hankel function whose asymptotic form closely matches the ray structure of the slab mode in the common region between the slab and wedge. Interpreting this asymptotic solution in terms of rays leads to a ray-tracing procedure whereby rays are multiply reflected from the wedge walls. The amplitude and phase of the reflected ray fields are assumed to be altered by Fresnel reflection coefficients. From this ray field an approximate expression for the actual field on the wedge surface is then formulated in terms of a series of integrals whose integrands contain saddle points or stationary phase points associated with these ray trajectories (i.e., are obtained from saddle point conditions which specify the ray structure). Very little numerical data was obtained due to limited computational capability and a non-optimal choice of

-2-

complex integration paths. Furthermore, the tangential magnetic field on the wedge surface and the far fields were not formulated. After elucidating and extending the theory to include all tangential field components on the wedge surface and formulating a more efficient numerical scheme which reduced computational time by one-to-two orders of magnitude, the wedge's surface field and directive gain were shown to possess appropriate physical characteristics. These include wedge surface fields whose intensities peak while phase variations indicate the launching of radiation and end-fire radiation patterns which become more directive as the wedge length, relative to wavelength, is increased.

Since we are interested in a dielectric slab waveguide feeding a dielectric wedge antenna, the modal solution of the infinite dielectric slab is relevant and is reviewed in Section 2. In Section 3, a ray-optical solution in a wedge geometry is presented. It is necessary to be familiar with this solution in order to understand the construction, in Section 4, of the plane wave integral representation for the field in a dielectric wedge. Numerical results are discussed in Section 5, wherein comparisons are made between the above plane wave integral approach, the local mode approach of Schering [11], and experimental near field measurements made by Maurer and Gopen [21].

2. THE DIELECTRIC SLAB

Since the intended purpose of this study is to examine the guidance and radiation properties of a dielectric wedge fed by a dielectric slab waveguide, it is convenient, first, to review the field structure of the infinite dielectric slab in detail.

Exact Modal Solution

The guided mode structure of the dielectric slab waveguide is well known [22,23]. Consequently, pertinent results will be presented without detailed derivations. The geometry of an infinite slab waveguide is depicted in Fig. 1. Region A ($|x| < d$, $|y| < \infty$) is occupied by a non-magnetic dielectric of relative permittivity ε_r while regions $B^{\pm}$ ($|x| > d$, $|y| < \infty$) are free space. Since the geometry is invariant with the z-coordinate, the spatial dependency of the source free field structure it supports is taken to be independent of the z-direction. A time dependence of $\exp[-i\omega t]$ is assumed and suppressed. Of interest is the lowest order even TE – mode.

For modes TE to y, Maxwell's field equations yield the component set (E_z, H_x, H_y). The electric field component satisfies the two-dimensional reduced wave equation

$$(\frac{\partial^2}{\partial x^2} + \frac{\partial^2}{\partial y^2} + k_o^2 \varepsilon_r) \, E_z(x,y) = 0 \qquad (2.1)$$

while the magnetic field components follow from the relations

$$H_x = \frac{1}{i\omega\mu_o} \frac{\partial E_z}{\partial y} \quad , \qquad H_y = \frac{-1}{i\omega\mu_o} \frac{\partial E_z}{\partial x} \qquad (2.1a)$$

-4-

The wavenumber $k = \omega \sqrt{\mu_o \epsilon_o \epsilon_r}$ reduces to the free space wavenumber when ϵ_r, the relative dielectric constant, is unity; μ_o and ϵ_o are the permeability and permittivity of free space. Using the method of separation of variables and considering waves travelling in the +y-direction only, we obtain as a solution to (2.1) the electric field in the dielectric ($|x| < d$) to be:

$$E_z = A \cos(k_x x) e^{ik_y y}$$

$$H_x = \frac{k_y}{\omega\mu_o} A \cos(k_x x) e^{ik_y y} \qquad (2.2)$$

$$H_y = \frac{k_x}{i\omega\mu_o} A \sin(k_x x) e^{ik_y y}$$

where

$$k_x^2 + k_y^2 = k^2 = \omega^2 \mu_o \epsilon_o \epsilon_r \qquad (2.2a)$$

while the field structure in free space ($|x| > d$) can be shown to take the form

$$E_z = A \cos(k_x d) e^{-\alpha_x(|x|-d)} e^{ik_y y}$$

$$H_x = \frac{k_y}{\omega\mu_o} A \cos(k_x d) e^{-\alpha_x(|x|-d)} e^{ik_y y} \qquad (2.3)$$

$$H_y = \frac{x}{|x|} \frac{\alpha_x}{i\omega\mu_o} A \cos k_x d \; e^{-\alpha_x(|x|-d)} e^{ik_y y}$$

with

$$-\alpha_x^2 + k_y^2 = k_o^2 = \omega^2 \mu_o \epsilon_o \qquad (2.3a)$$

-5-

The amplitude constants of E_z in (2.2) and (2.3) have been chosen to satisfy continuity of the E_z component across the air-dielectric interfaces at $x = \pm d$. Continuity of the tangent magnetic field components H_y at $x = \pm d$ yields the eigenvalue equation

$$\tan k_x d = \frac{\alpha_x}{k_x} \qquad (2.4)$$

In addition, the above continuity conditions require the y-directed propagation constant k_y in the dielectric and in the free space to be identical.

By replacing the cosine function in (2.2) by exponential functions, the field solution can then be interpreted as a superposition of the two plane waves, one progressing upward toward the interface at $x = + d$ and the other progressing downward toward the interface at $x = - d$. Hence, we may write

$$E_z = E_z^+ + E_z^- ,$$

with $\qquad (2.5)$

$$E_z^{\pm} = (A/2) \; e^{\pm i k_x x + i k_y y}$$

It is apparent from (2.2a) that these plane waves impinge on the interfaces at angles w^i, measured relative to a surface normal, given by

$$\tan w^i = k_y/k_x \qquad (2.6)$$

Since the modal field takes the form of a superposition of two plane waves, one incident and the other reflected from the air-dielectric

-6-

boundaries, it is quite natural to introduce reflection coefficients $\Gamma^{\pm}$
at both the upper (+) and lower (-) walls of the slab. Thus, at $x = d$,
(2.5) gives the reflection coefficient

$$\Gamma^+ \equiv E_z^- / E_z^+ = e^{-i2k_x d} = \Gamma^- \qquad (2.7)$$

From (2.4) and (2.7), it then follows that

$$\Gamma^- = \Gamma^+ = \frac{1 - j\alpha_x / k_x}{1 + j\alpha_x / k_x} , \qquad (2.8)$$

which by using (2.2a), (2.3a), and (2.6) yields the Fresnel reflection
coefficient for a perpendicularly polarized incident plane wave

$$\Gamma^+ = \Gamma^- = \frac{\cos w^i - \sqrt{1/\varepsilon_r - \sin^2 w^i}}{\cos w^i + \sqrt{1/\varepsilon_r - \sin^2 w^i}} \qquad (2.9)$$

The eigenvalue equation (2.4) specifies discrete values for the
separation constants k_x, k_y and α_x, which in turn yields from (2.6) dis-
crete propagation direction angle w^i. By combining (2.2a) and (2.3a) with
the eigenvalue equation (2.4), it follows that $k_x d$ satisfies the relation-
ship

$$(k_x d)^2 \sec^2 (k_x d) - (k_o d)^2 (\varepsilon_r - 1) = 0 . \qquad (2.10)$$

Since we are interested in single mode propagation, the first zero of
(2.10) is needed and was found by using the Newton-Raphson method.

One can show that the exact modal solution given by (2.2) can be de-
rived using the concepts of ray optics [16,18,24], which are formally pre-
sented in Appendix A. For propagating in the +y direction, the ray-optical
solution takes the form of the two plane waves of equal amplitude given by

-7-

eq. (2.5). The ray structure in the slab is depicted in Fig. 2, wherein rays progressing toward the upper wedge wall ($x = d$) are identified by the normalized phase function S_1 and the rays progressing toward the bottom wall are identified by the phase S_2 (see Appendix A).

3. THE DIELECTRIC WEDGE

While ray optical and full wave solutions are identical for the dielectric slab problem, such agreement is not attained for the dielectric wedge. Maurer and Felsen [16] have effected ray solutions for the wedge geometries which possess constant surface reflection coefficients. This enabled the eiconal equation of ray optics (see eq.(A4)) to be solved by the separation of variable technique, as was done for the dielectric slab [16,24]. Unfortunately, this constraint on the reflection coefficient is not physically realizable for the dielectric wedge. In the wedge, complex diffraction fields of the same order of magnitude as the ray optical fields occur. These diffraction effects are due to the occurrence in the integral representation of double saddle points and multiple branch points, which are closely related to caustics and multiply-reflected lateral waves. A caustic is an envelope of a system of real rays. Lateral waves are waves that transmit energy along a boundary between two media when a wave in the optically-denser side hits the interface at the critical angle; as the wave travels parallel to the boundary in the optically-thinner medium, it sheds energy back into the optically-denser material by refraction [25].

It has been recognized that the simpler approach of ray optics can provide important, though incomplete, information about asymptotic fields. Constructs of ray optics and results of a full-wave analysis are rigorously related [27]. In particular, the ray fields provide arguments of the functions that enter into the uniformly asymptotic descriptions of exact field solutions. Thus, the method of ray optics provides a convenient starting point for studying the wave guidance and radiation properties of the dielectric wedge. Consequently, a review of the ray optical solution is warranted.

-9-

w with these ray trajectories such that $\cos w = a/r$. For observation points $r < a$, no real rays exist. In this region we have complex evanescent ray solutions [16]. By requiring wedge rays at $r = r_T$, $\theta = 0$, i.e., at the interface between the slab and the wedge to evolve continuously from corresponding slab rays of incidence angle $w = w^i = w_T$ (see Fig. 3 and eq. (2.6)), geometric construction stipulates that

$$w_T = \cos^{-1}(a/r_T) \ . \tag{3.8}$$

It is apparent that each modal solution in the slab corresponds to a set of rays in the wedge where each set is associated with an eigenvalue $a = a_m$ which defines a cylindrical caustic $r = a_m$. Since we are considering only the lowest order mode in the slab, we need only consider one modal set in the wedge or $a = r_T \cos w_T$.

To complete the ray optical description of the field structure in a dielectric wedge with surface impedances which insure constant reflection coefficients, the amplitudes of the wedge rays must be ascertained. These amplitudes were found by requiring either conservation of energy in a ray tube [20,24] or by solving the lowest order transport equation (A5) [16]. Considering only rays propagating in the $(-r)$ direction, i.e., toward the tip and assuming $C_1 = -C_2 = C$ in (3.5), the electric field can then be shown to be expressed by

$$E_z = E_z^+ + E_z^-$$

where

$$E_z^\pm \simeq \frac{A}{(r^2 - a^2)^{\frac{1}{4}}} \ e^{-jk\left[(r^2 - a^2)^{\frac{1}{2}} - a\cos^{-1}(a/r)\right] \pm jk(a\theta + c)} \tag{3.9}$$

-11-

The eigenvalues $a = a_m$ are specified by (3.6) and are related to slab ray

directions by (3.8). The arbitrary constant c in (3.9) follows directly

by requiring continuity of phase across the transition region at $r \tilde{=} r_T$,

$\theta = 0$ in the limit of small β (see Fig. 3).

B.   Plane Wave Integral Solutions When Reflection Coefficients Are
       Angular Dependent

A modal ray description of the field in a dielectric wedge with constant

reflection coefficients at the air-dielectric interfaces and for propagation

towards the tip in the region $r_T \leq r < a$, $-\beta/2 \leq \theta \leq \beta/2$ has been obtained

(see 3.9). It is apparent from (3.9) that the field amplitude and hence

energy density become infinite as $r \to a$. This behavior is also indicated

by the convergence of ray tubes at the cylindrical caustics $r = a_m$. Thus,

simple geometric optic arguments break down and indicates that a more uniformly

asymptotic formulation of the modal field solution in the wedge is required.

In the integral formulation by Maurer and Siwiak [19,20], multiple la-

teral wave-type diffraction effects are indicated by the occurrence of multiple

branch points in the angularly dependent reflection coefficients. Attempting

to isolate the individual lateral waves and their reflections was not possible

since the interaction of the branch point effects was found to be important,

i.e., they could not be treated as isolated branch points. The overall effect

could only be accounted for by numerical integration techniques. A reformula-

tion of these plane wave integral representations is given below.

To justify the postulated form of the integral representations for

the modal field on the surface of a dielectric wedge (see (3.34) and (3.35)),

consider two plane wave solutions to the two-dimensional scalar wave equa-

tion which are assumed to propagate in the +y direction.

-12-

$$E_z = E_z^+ + E_z^- = (A^+ e^{jk_x x} + A^- e^{-jk_x x}) e^{jk_y y} \tag{3.10}$$

where $k_y = \sqrt{k^2 - k_x^2} > 0$. By transforming this solution into polar coordinates via the relations

$$x = r \cos\phi \qquad\qquad y = r \sin\phi$$

$$k_x = k \cos\alpha \qquad\qquad k_y = k \sin\alpha$$

we obtain

$$E_z = E_z^+ + E_z^- = A^+ e^{-jkr \cos(\Pi+\alpha-\phi)} + A^- e^{-jkr \cos(\alpha+\phi)} \tag{3.11}$$

Eq. (3.11) represents two plane waves which progress in the directions $\phi = \Pi + \alpha$ and $\phi = -\alpha$ toward the origin* in xy-space, respectively.

A more general solution to the wave equation can be constructed by superposition [26]. Hence, we may write

$$E_z^+ = \int_{\alpha_1}^{\beta_1} A^+(\alpha)\, e^{-jkr \cos(\Pi+\alpha-\phi)} d\alpha \tag{3.12a}$$

and

$$E_z^- = \int_{\alpha_2}^{\beta_2} A^-(\alpha)\, e^{-jkr \cos(\alpha+\phi)} d\alpha \tag{3.12b}$$

with $A^{\pm}(\alpha)$ an analytic function dependent on α. E_z^+ represents a bundle of plane waves propagating in the directions $\alpha_1 \leq \alpha \leq \beta_1$ toward the upper wedge air-dielectric interface; E_z^- identifies a set of plane waves progressing toward the lower wedge wall in the directions $\alpha_2 \leq \alpha \leq \beta_2$.

---

*Specification of wave motion toward the origin is relevant in polar coordinates since our main concern is with the effects of wave guidance toward the tip of the wedge.

-13-

In an unbounded domain, solutions to the wave equation in polar coordinates are of the form [26]

$$E_z = Z_\nu \ (kr) \ e^{i\nu\phi} \ , \tag{3.13}$$

where ν is a separation constant and $Z_\nu(kr)$ represents a general cylinder function. For waves approaching the origin, Z_ν becomes a Hankel function of the second kind whose integral representation in the complex w'-space is

$$H_{ka}^{(2)}(kr) = \frac{1}{\Pi} \int_{P_2} e^{+ikr \cos w'} \ e^{ika(w' - \Pi/2)} \ dw' \tag{3.14}$$

where ν has been set equal to ka and the path P_2 is defined in Fig. 5.

The ray optical interpretation of the asymptotic form of solution (3.13) with Z_ν given by (3.14) and ν-positive is depicted in Fig. 6. As illustrated, rays are trajectories orthogonal to the wave fronts and tangent to the circular caustic $r = a$. Since our wave bundles (3.12) also approach the origin and we expect product separability as in (3.13), let us assume that the angular dependent coefficients in E_z can be expressed as

$$A^{\pm}(\alpha) = B^{\pm} \ e^{jka(\alpha-\Pi/2)} \ , \ B^{\pm} \ \text{independent of } \alpha. \tag{3.15}$$

Substitution of (3.15) into (3.12a) and (3.12b) gives

$$E_z^+ = B^+ \int_{\alpha_1}^{\beta_1} e^{-jkr \cos(\Pi+\alpha-\phi) + jka(\alpha-\Pi/2)} \ d\alpha \tag{3.16a}$$

$$E_z^- = B^- \int_{\alpha_2}^{\beta_2} e^{-jkr \cos(\alpha+\phi) + jka(\alpha-\Pi/2)} \ d\alpha \tag{3.16b}$$

-14-

From Fig. 3, it is clear that the coordinate θ is more convenient than the ϕ coordinate. Setting $\theta = \phi - 3\Pi/2$ reduces (3.16a) and (3.16b) to

$$E_z^+ = B^+ \int_{\alpha_1}^{\beta_2} e^{-jkr \sin(\alpha-\theta) + jka(\alpha-\Pi/2)} d\alpha \tag{3.17a}$$

$$E_z^- = B^- \int_{\alpha_2}^{\beta_2} e^{-jkr \sin(\alpha+\theta) + jka(\alpha-\Pi/2)} d\alpha \tag{3.17b}$$

As in (3.13), the θ-dependence can be isolated by introducing the transformations $w = \alpha - \theta$ in E_z^+ and $w = \alpha + \theta$ in E_z^-; hence

$$E_z^+ = B^+ e^{-jka(\Pi/2-\theta)} \int_{\alpha_1-\theta}^{\beta_1-\theta} e^{-jkr \sin w + jka w} dw \tag{3.18a}$$

and

$$E_z^- = B^- e^{-jka(\Pi/2+\theta)} \int_{\alpha_2+\theta}^{\beta_2+\theta} e^{-jkr \sin w + jka w} dw \tag{3.18b}$$

At the upper wedge wall, i.e., when $\theta = \beta/2$, the ray bundle E_z^+ in (3.18) reflects into the ray bundle E_z^- as shown in Fig. 7. From the geometry we see that α varies in (3.18a) between $\alpha_1 = w_T - \beta/2$ and $\beta_2 = w_T + \beta/2$, where w_T is equal to the angle of incidence of the plane waves in the slab, and in (3.18b) between $\alpha_2 = w_T - \frac{3\beta}{2}$ and $\beta_2 = w_T - \frac{\beta}{2}$. Hence over region 1, (see Fig. 7 for specification of region 1 on the upper wedge wall), the field is given by

$$E_{z1} = E_{z1}^+ + E_{z1}^- \tag{3.19}$$

where

-15-

$$E_{z1}^+ = B^+ \, e^{-jka(\Pi-\beta)/2} \int_{\theta_T-\beta}^{\theta_T} e^{jkaw - jkr \sin w} \, dw \qquad (3.19a)$$

and

$$E_{z1}^- = B^- \, e^{-jka(\Pi+\beta)/2} \int_{\theta_T-\beta}^{\theta_T} e^{jkaw - jkr \sin w} \, dw \qquad (3.19b)$$

Furthermore, $B^+ = B^-$. This follows from symmetry by noting that, for ex-
citation of the wedge by a symmetric slab mode, the field over the top and
bottom surfaces of the wedge ($\theta = +\beta/2$ and $-\beta/2$, respectively) must be iden-
tical. Consequently, the incident wave bundle E_{z1}^+ illuminating region 1 on
the upper wedge surface equals the field E_{z1}^- which illuminates region 1 on
the lower wedge surface, and both are superpositions of plane waves which
span the angular range $w_T - \beta/2 < w < w_T + \beta/2$. Hence, from eqs. (3.18a)
and (3.18b), $B^+ = B^- = B_1$ and we may write for the field over region 1 on
the upper wedge wall $(\theta = \beta/2)$:

$$E_{z1} = B_1 \, e^{-jka(\Pi-\beta)/2} \left[\int_{\theta_T-\beta}^{\theta_T} (1 + \Gamma_1^+) \, e^{jkW(w)} \, dw \right] \qquad (3.20)$$

where the reflection coefficient on the upper wedge wall is given by

$$\Gamma_1^+ = E_{z1}^- / E_{z1}^+ = e^{-jka\beta} \equiv \Gamma_T \qquad (3.21a)$$

and

$$W(w) = aw - r \sin w \qquad (3.21b)$$

Eq. (3.21a) also follows from the modal resonance relation (3.6) for the
lowest order mode ($m = 0$). Furthermore, for small apex angles β it follows
from (3.8) and the relationship $\sin \beta/2 \simeq \beta/2 = d/r_T$ that expression (3.21a)

-16-

reduces to eq. (2.7) with $\Gamma^{\pm}$ given by the Fresnel polarization dependent reflection coefficient (2.9).

The integral representations for the magnetic field components follow directly from Maxwell's source free equations

$$H_r = \frac{1}{j\omega\mu_o} \frac{1}{r} \frac{\partial}{\partial\theta} E_z \quad , \quad H_\theta = -\frac{1}{j\omega\mu_o} \frac{\partial}{\partial r} E_z \tag{3.22}$$

Applying (3.22) to the integrals (3.17a) and (3.17b) and following the same procedure which led to obtaining (3.18a) and (3.18b) results in giving for the magnetic field components

$$H_r = H_r^+ + H_r^- \quad , \quad H_\theta = H_\theta^+ + H_\theta^- \tag{3.23}$$

with

$$H_r^+ = -\left(\frac{B^+}{\eta} \int_{\alpha_1-\theta}^{-\beta_1-\theta} \cos w \; e^{jkW(w)} \; dw \right) e^{-jka(\Pi/2-\theta)} \tag{3.23a}$$

$$H_r^- = \left(\frac{B^-}{\eta} \int_{\alpha_2+\theta}^{-\beta_2+\theta} \cos w \; e^{jkW(w)} \; dw \right) e^{-jka(\Pi/2+\theta)} \tag{3.23b}$$

and

$$H_\theta^+ = \left(\frac{B^+}{\eta} \int_{\alpha_1-\theta}^{-\beta_1-\theta} \sin w \; e^{jkW(w)} \; dw \right) e^{-jka(\Pi/2-\theta)} \tag{3.23c}$$

$$H_\theta^- = \left(\frac{B^-}{\eta} \int_{\alpha_2+\theta}^{\beta_2+\theta} \sin w \; e^{jkW(w)} \; dw \right) e^{-jka(\Pi/2+\theta)} \tag{3.23d}$$

where $W(w)$ is given by (3.21b). Hence, for $\theta = \beta/2$ and illumination over region 1, (3.23) reduces to

-17-

$$H_{r1} = \frac{B_1}{\eta} e^{-jka(\Pi-\beta)/2} \int_{w_T-\beta}^{w_T} \cos w \, [1 - \Gamma_1^+] \, e^{jkW(w)} \, dw \qquad (3.24a)$$

and

$$H_{\theta 1} = \frac{B_1}{\eta} e^{-jka(\Pi+\beta)/2} \int_{w_T-\beta}^{w_T} \sin w \, [1 + \Gamma_1^+] \, e^{jkW(w)} \, dw \qquad (3.24b)$$

where use was made of the fact that $B^+ = B^- = B_1$.

The surface field components specified by (3.20) and (3.24), however, do not represent the actual physical situation. If we now assume that the reflection coefficient is angular dependent and given by (2.9) with w^i replaced by w, we may rewrite (3.20) and (3.24) as

$$E_{z1} = B_1 e^{-jka(\Pi-\beta)/2} \int_{w_T-\beta}^{w_T} [1 + \Gamma(w)] \, e^{jkW(w)} \, dw \qquad (3.25a)$$

$$H_{r1} = \frac{B_1}{\eta} e^{-jka(\Pi-\beta)/2} \int_{w_T-\beta}^{w_T} \cos w \, [1 - \Gamma(w)] e^{jkW(w)} \, dw \qquad (3.25b)$$

and

$$H_{\theta 1} = \frac{B_1}{\eta} e^{-jka(\Pi-\beta)/2} \int_{w_T-\beta}^{w_T} \sin w \, [1 + \Gamma(w)] e^{jkW(w)} \, dw \qquad (3.25c)$$

The integral expression (3.25a) agrees with eq. (42) of [24], which was derived by inferring the integral expression from a ray optical development whereas in (3.25) the development follows from a finite superposition of plane waves following the ray trajectories.

In order to understand how the signal illuminates the entire wedge surface, it is necessary to track the wave bundles as they progress along

-18-

the wedge toward the apex. Consider the situation of once reflected beams and illumination of region 2 on the wedge air-dielectric interface (see Fig. 7). From geometric construction, upgoing plane waves E_{z2}^+ which illuminate region 2 are confined to the angular directions $w_T - 3\beta/2 < \alpha < w_T - \beta/2$, whereas reflected waves E_{z2}^- are confined to the directions $w_T - 5\beta/2 < \alpha < w_T - 3\beta/2$. As a consequence, eqs. (3.18a) and (3.18b) take the form

$$E_{z2}^+ = B_2^+ \ e^{-jka(\Pi-\beta)/2} \int_{w_T-2\beta}^{w_T-\beta} e^{jkW(w)} \ dw \qquad (3.26a)$$

and

$$E_{z2}^- = B_2^- \ e^{-jka(\Pi+\beta)/2} \int_{w_T-2\beta}^{w_T-\beta} e^{jkW(w)} \ dw \qquad (3.26b)$$

where $W(w)$ is given by (3.21b). Hence, at $\theta = \beta/2$ along region 2 in Fig. 7, the surface illumination from the beam progression toward the tip is given by

$$E_{z2} = E_{z2}^+ + E_{z2}^- = B_2 \ e^{-jka(\Pi-\beta)/2} \int_{w_T-2\beta}^{w_T-\beta} (1 + \Gamma_2^+) \ e^{jkW(w)} dw \qquad (3.27)$$

with reflection coefficient Γ_2^+ given by

$$\Gamma_2^+ \equiv E_{z2}^-/E_{z2}^+ = e^{-jka\beta} \equiv \Gamma_T \qquad (3.27a)$$

and symmetry requiring that $B_2^+ = B_2^- = B_2$.

In order to relate B_2 to B_1, the observation is made that E_{z1}^- waves incident on region 1 of the lower wedge air-dielectric interface span the angular directions $w_T - \beta/2 < \alpha < w_T + \beta/2$ and reflect as E_{z2}^+ in direction

-19-

$w_T - 3\beta/2 < \alpha < w_T - \beta/2$. Thus, at $\theta = -\beta/2$,

$$E_{z1}^{-} = B_1 \, e^{-jka(\Pi-\beta)/2} \int_{w_T-\beta}^{w_T} e^{jkW(w)} \, dw \qquad (3.28a)$$

and

$$E_{z2}^{+} = B_2 \, e^{-jka(\Pi-\beta)/2} \int_{w_T-\beta}^{w_T} e^{jkW(w)} \, dw \qquad (3.28b)$$

The reflection coefficient along region 1 of the lower air-dielectric interface is now defined as

$$\Gamma_1^{-} = E_{z2}^{+}/E_{z1}^{-} = B_2 \, e^{-jka\beta}/B_1 = B_2\Gamma_T/B_1 \, . \qquad (3.29)$$

where Γ_T has been introduced in (3.21a). On replacing B_2 in (3.28b) by using (3.29) and combining E_{z2}^{+} with E_{z1}^{-}, one obtains for the surface field along region 2 on the upper wedge wall the expression

$$E_{z2} = B_1 \, e^{-jka(\Pi-\beta)/2} \int_{w_T-2\beta}^{w_T-\beta} \frac{\Gamma_1^{-}(1 + \Gamma_1^{+})}{\Gamma_T} \, e^{jkW(w)} \, dw \qquad (3.30)$$

Again allowing the reflection coefficients to be angular dependent and observing that if $\Gamma_1^{+} = \Gamma(w)$ then Γ_1^{-} must equal $\Gamma(w + \beta)$, eq. (3.30) becomes

$$E_{z2} = B_1 \, e^{-jka(\Pi-\beta)/2} \int_{w_T-2\beta}^{w_T-\beta} \frac{\Gamma(w + \beta)}{\Gamma_T} \, [1 + \Gamma(w)] \, e^{jkW(w)} \, dw \qquad (3.31)$$

where $\Gamma(w)$ is given by (2.9) with w_i replaced by w.

By continuing the above process of tracking beam reflections from the wedge walls, it evolves that the surface field along the nth region

-20-

of the upper wedge wall can be approximated by the integral expression

$$E_{zn} = B_1 \ e^{-jka(\Pi-\delta)/2} \int_{w_T-n\delta}^{w_T-(n-1)\delta} [1+\Gamma(w)] \prod_{m=1}^{n-1} \frac{\Gamma(w + m\delta)}{r_T^{n-1}} e^{jkW(w)} dw \qquad (3.32)$$

Thus, along the plane $\theta = \delta/2$ between the apex $r = 0$ and the transition region $r = r_T$, the surface electric field is given by

$$E_z = \sum_{n=1}^{N} E_{zn} \ . \qquad (3.33)$$

where E_{zn} is specified by (3.32) and $w_T = N\delta$. The integer N identifies the number of regions along the upper wedge wall that are directly illuminated by the plane waves as they progress toward the tip and are multiply reflected from the wedge air-dielectric interface. Note that when $n = N$, $w = w_T - n\delta = 0$; hence, the final wave constituent in E_{zn} is normally incident on the upper wedge wall. As was pointed out in [24], this plane wave is tangent to the caustic at $r = a$, $\theta = \delta/2$.

For $n > N$, the integral (3.32) describes surface illumination for waves progressing back toward the slab region. When $n = 2N$, $w = -w_T$; the associated plane wave constituent illuminates region 1 on the upper wedge wall at observation point $(r_T, -\Pi/2)$ and is incident at an angle of $-w_T$ measured to the right of a unit normal to the wedge wall [24]. Hence, the surface illumination considering both right-going and left-going waves is given by the expression

$$E_z = \sum_{n=1}^{2N} E_{zn} \ , \qquad \theta_T = N\delta \ . \qquad (3.34)$$

which results in integers being evaluated numerically between the limits

-21-

$-w_T < w < w_T.$

The remaining field components can be inferred from (3.25) and (3.32). Hence,

$$H_r = \sum_{n=1}^{2N} H_{rn} \quad , \qquad H_\theta = \sum_{n=1}^{2N} H_{\theta n} \tag{3.35}$$

with

$$H_{rn} = \frac{B_1}{\eta} e^{-jka(\Pi-\beta)/2} \int_{w_T-n\beta}^{w_T-(n-1)\beta} \cos w \, [1 - \Gamma(w)] \prod_{m=1}^{n-1} \frac{\Gamma(w+m\beta)}{\Gamma_T^{n-1}} e^{jkW(w)} \, dw \tag{3.35a}$$

and

$$H_{\theta n} = \frac{B_1}{\eta} e^{-jka(\Pi-\beta)/2} \int_{w_T-n\beta}^{w_T-(n-1)\beta} \sin w \, [1 = \Gamma(w)] \prod_{m=1}^{n-1} \frac{\Gamma(w+m\beta)}{\Gamma_T^{n-1}} e^{jkW(w)} \, dw \tag{3.35b}$$

The above expressions, eqs. (3.34) and (3.35), are assumed to give the surface field at observation points $r < a$, i.e., in the region shielded by the caustic. The justification for this assumption is that complex diffraction effects take place when the incidence angle w passes the critical angle θ_c, which is given by $\theta_c = \sin^{-1}(1/\sqrt{\varepsilon_r})$ and corresponds to a branch point. The integration paths of (3.34) and (3.35) encounter multiple branch points that are introduced by the multiple reflection coefficients in the integrand. These branch points establish lateral wave-types that constitute the dominant field within the caustic [24].

Although the integration paths lie in the range $-w_T < w < w_T$, numerical evaluation of (3.34) and (3.35) as well as experimental evidence have indicated that no measurable energy is reflected back into the slab. This

-22-

results because the reflection coefficients have magnitudes less than or equal to unity and as more and more of these are included in the integrand, they reduce its magnitude rapidly after the critical angle has been passed.

4.   THE FAR FIELD

Using the theory presented in Section 3, the tangential electromag-
netic field components can be calculated at a suitable number of points
along the surface of a given wedge. From the results of Section 2, the
evanescent field external to the slab can be determined along a hypothetical
wedge boundary extending out to infinity radially, as diagramatically il-
lustrated in Fig. 8. These radial lines, in conjunction with a circular
path at infinity, enclose a domain D, occupied by free space which is
external to the dielectric slab-wedge radiator. Since domain D contains
no sources, Kirchhoff-Huygen diffraction integral can be applied to find
the fields radiated into the region D in terms of the tangential fields
on the boundary of D, designated ∂D_i, i = 1,2 and ∞, in Fig. 8.

In free space, the radiated electromagnetic field, $E_z(\underline{r})$ satisfies
the two-dimensional wave equation:

$$(\nabla^2 + k_o^2) \quad E_z(\underline{r}) \; = \; 0 \tag{4.1}$$

where $E_z(\underline{r})$ is the radiated field, $\underline{r}$ is the position vector to some point
P in D where the far field is to be determined, and k_o is the free space
wave number.   Let G_o satisfy the equation

$$(\nabla^2 + k_o^2) \quad G_o(\underline{r}, \underline{r}') \; = \; - \, \delta(\underline{r} - \underline{r}') \tag{4.2}$$

where $\delta(\underline{r} - \underline{r}')$, the Dirac Delta function, represents an infinitessimal
point source of unity magnitude at $\underline{r} = \underline{r}'$.   By first multiplying (4.1)
by G_o and (4.2) by $-E_z(\underline{r}')$, subtracting the two, then integrating the re-
sultant expression over the surface enclosing D and using Green's second

-24-

identity in two dimensions, it evolves that the far field can be obtained
from the expression

$$E_z(\underline{r}) = \oint_C [G_o(\underline{r},\underline{r}') \frac{\partial E_z(\underline{r}')}{\partial n} - E_z(\underline{r}') \frac{\partial G_o(\underline{r},\underline{r}')}{\partial n}] \, d\ell' ,$$ (4.3)

where $\hat{\underline{n}}$ is the unit normal to the curve C pointing into the enclosed area D
and $d\ell'$ is an element of arc length on C. Clearly, (4.3) is an integral
solution for the far field $E_z(\underline{r})$ in terms of the boundary values $E_z(\underline{r}')$
and the Green's function $G_o(\underline{r},\underline{r}')$. Since the two-dimensional radiation
condition ensures that the contribution from the boundary of D at infinity
vanishes and since the evanescent field decays very rapidly along the hypo-
thetically extended wedge surface, the integral (4.3) needs to be evaluated
only a short distance past the interface between the wedge and the slab.

The solution to (4.2) is a Hankel function of the first kind [25]

$$G_o = \frac{1}{4} H_o^{(1)}(k_o R), \quad R = |\underline{r} - \underline{r}'|,$$ (4.4)

which in the far field (large $k_o R$) asymptotically reduces to

$$G_o(\underline{r},\underline{r}') = \frac{1}{2} \frac{e^{j(k_o R + \pi/4)}}{(2\pi k_o R)^{\frac{1}{2}}}$$ (4.5)

Since in the far field $\underline{R}$ is approximately parallel to $\underline{r}$, it follows
from geometrical considerations (see Fig. 8) that

$$R \simeq r + r' \cos(\xi + \beta/2) = r + r' \sin(u),$$ (4.6)

where ξ is the angle measured from the forward direction, i.e., from the
positive y axis, β is the apex angle of the wedge, and u is the angle

-25-

between the normal $\hat{\underline{n}}$ to the wedge surface and position vector $\underline{R}$. The normal derivative of the Green's function can then be shown to take the form

$$\frac{\partial G_o}{\partial n} = -\frac{1}{r} \frac{\partial G_o}{\partial \phi} \sim - k_o \cos(u) G_o \qquad (4.7)$$

with G_o given by the asymptotic form (4.5).

From Maxwell's equation in cylindrical coordinates, the normal derivative of the tangential electric field is related to the tangential magnetic field by the expression

$$\frac{\partial E_z}{\partial n} = \hat{\underline{n}} \cdot \nabla E_z = \frac{1}{r} \frac{\partial E_z}{\partial \phi} = -j\omega\mu_o H_r \qquad (4.8)$$

Combining (4.7) and (4.8) with (4.3) gives the radiated far electric field

$$E_z(\underline{r}) \sim \int_{\partial D_1 \text{ and } \partial D_2} jk_o G_o \; [\cos(u)E_z - \eta_o H_r] \quad dr' \qquad (4.9)$$

In (4.9), the integration ranges over the two segments ∂D_1 and ∂D_2 defined in Fig. 8, G_o is given by (4.5) and (k_o, η_o) are the wavenumber and the intrinsic wave impedance of free space. The integration of (4.9) is carried out along both wedge surfaces. As will later be discussed in greater detail, Romberg's method was employed in the analysis of actual wedge problems.

-26-

5. NUMERICAL RESULTS

The wedge antenna is completely characterized by three parameters: $k_o d$. the relative half-width of the slab with respect to the free space wavenumber k_o, $k_o \ell$, the relative length of the wedge and ε_r, the relative permittivity of the antenna material. These values are varied so as to determine the effect each has on both the surface field and the far field. In addition, surface and far fields are calculated for two antennas with a relative permittivity of silicon, $\varepsilon_r = 12$. For these two antennas, our theoretical results are compared with an alternative approach based on the local mode theory [11]. The silicon material with $\varepsilon_r = 12$ is currently under study for use in millimeter-wave transmitters and receivers being developed by the U.S. Army. The antenna parameters examined are listed in Table 1, with identifying letters A through L. Also included in this table are the values of w_T, β and $k_o a$. The angle w_T is the incident angle for the plane waves in the slab which excite the wedge. Recall that the range $-w_t \leq w \leq w_T$ specifies the integration limits for the wedge surface fields. The parameter β is the apex angle of the wedge and $k_o a$ is the location of the caustic relative to the free space wavenumber. Antennas J, K, and L are of particular interest because of the availability of empirical data collected by Maurer and Gopen [21]. The material used in the experiment was rexolite with a relative permittivity $\varepsilon_r = 2.56$.

In Section 4 and in eq. (4.9) it was shown that a far field evaluation requires first calculating the field components E_z and H_r along the planar surfaces ∂D_1 and ∂D_2, identified in Fig. 8. Physically, these surface field components must be continuous along ∂D_1 and ∂D_2. Hence, we imposed the con-

-27-

dition that the electric field on the surface of the dielectric wedge be equal to the electric field in the evanescent region of the slab waveguide at the trnasition point $r = r_T$, $\theta = \beta/2$, i.e., we equated (3.33) to (2.3). The small discontinuity in H_r across the transition point was found to be acceptable (see, for example, Fig. 13 through Fig. 16). In addition, it was convenient to normalize the surface wedge field by setting the multiplicative factor in (3.32), $B_1 \exp [-jka(\Pi - \beta/2)]$, to unity.

A.   The Surface Field

The relative magnitude (in dB) of the surface electric and magnetic tangent fields as well as their respective phases are plotted versus the normalized coordinate $k_o y'$ in Figs. 9-16. Values are plotted from the tip $(k_o y' = k_o r_r)$, past the transition region $(k_o y' = 0)$ and extend into the evanescent region of the slab waveguide. The phase difference at the apex of each antenna is normalized to read 4Π radians. In Figs. 9a and 9b and Figs. 13a and 13b, the wedge length is increased while $k_o d$ and ε_r are held fixed. Figs. 10a and 10b, together with Figs. 14a and 14b show the effects of changing the relative slab width $k_o d$ while Figs. 11a and 11b, with Figs. 15a and 15b depict the surface field as ε_r is changed. In Figs. 16a and 16b, the surface field for two antennas with $\varepsilon_r = 12$ is presented. How these changes affect the far field will be discussed shortly.

Of particular interest is the phase velocity $v_{ph,y'}$ along the wedge surface in the y'-direction (forward direction). In order for a wave to be launched from the wedge in this direction, the corresponding component of the wavevector $k_{y'}$ must equal the free space wavenumber k_o (this follows from Snell's law). The wavevector $\underline{k}$ is defined as the spatial gradient of

-28-

the phase of the wave function (in our case, E_z). Since $k_{y'} = \hat{\underline{y}}' \cdot \underline{k}$,
where $\hat{\underline{y}}'$ is a unit vector in the positive y'-direction, we may formulate
the relation

$$k_{y'} - k_o = \frac{\partial}{\partial y'} (ARG(E_z) - k_o y')$$ (5.4)

where $y' = r_T - r'$. When this quantity is zero, the surface wave is launched.
Graphically, this is determined by plotting the function $Arg(E_z) - k_o y'$
and noting that when the slope is zero the surface wave enters the 'fast
wave' region and radiation becomes possible. This condition is illustrated
in Figs. 9b, 10b, 11b, and 12b.

B.   The Far Field

As the length $k_o \ell$ of the antenna is increased (see Figs. 9 and 12)
there results an expansion of the spatial interval on the surface of the
wedge over which the surface field has a phase velocity in the y'-direction
equal to the speed of light. Consequently, one expects enhanced radiation
capability. In Figs. 17 through 20, the directive gain g_d is plotted versus
the angle ξ, which is defined in Fig. 8. For two-dimensional geometries,
the directive gain is given by

$$g_d = 2\pi r S_r / P_{rad} ,$$ (5.5a)

where S_r is the real Poynting vector in the radial direction, expressed in
terms of the far electric field by $S_r = |E_z(\underline{r})|^2 / \eta_o$, $\eta_o = (\mu_o / \varepsilon_o)^{\frac{1}{2}}$ the
intrinsic impedance of free space, and P_{rad} is the power radiated by the
antenna. From Fig. 17, it appears that a larger value of $k_o \ell$ leads to more
power in the forward direction.

-29-

By decreasing the width $k_o d$ of the antenna, the endfire characteristics are also improved. Thus, in Fig. 18, antenna E has more directivity than either antenna C or D. This is most likely due to the fact that antenna E possesses a larger 'fast wave' region along the wedge surface than either antenna C or D, as is evident from Fig. 10b.

In Fig. 19, the relative permittivity ε_r is varied. Decreasing this parameter also increases the size of the fast wave region (see Fig. 11b) and thus antenna G has better propagating characteristics than either E or F.

Fig. 20 demonstrates that directive antennas could be designed with silicon ($\varepsilon_r = 12$); however, they would have to be very long or very narrow.

It was also observed that slightly changing the frequency, while not affecting the main beam, can increase or decrease the side and back lobes significantly, indicating that a more desirable combination of $k_o d$, $k_o \ell$, and ε_r can be found for a given application at a given frequency.

The directive gain for antennas H and I, with $\varepsilon_r = 12$, are compared to patterns generated by a local mode approach [11] in Fig. 20. In the end-fire direction, the two methods give comparable values for the gain function. When $|\xi| > 80^o$, the local mode theory yields results which decrease more rapidly than the plane waves approach; however, for these observation angles, the gain is already 20 dB below its maximum value.

In Figs. 21, 22, and 23, experimental results [21] are compared with theoretical ones. The normalized coordinate $k_o y'$ has its origin in the wedge surface at the transition region $r' = r_T$ (see Fig. 8) and is

-30-

directed toward the wedge tip. The parameter k_o is the free space wavenumber. The curves are normalized so that the experimental and theoretical values for the peak fields coincide. Near field experimental values were measured approximately one millimeter away from the wedge surface. The small fluctuations or ripples on the experimentally determined curves in Figs. 21-23 are most likely due to the presence of standing waves between the probe and the absorbing material surrounding the wedge and probe in the parallel-plate experimental setup [6]. As is evident from each of the figures, the experimental values dip downward across the transition region, while the theoretical values tend to tilt upward. There appears to be a discrepancy of about four to five dB between these two results. It ought to be pointed out that the location of the wedge, relative to the experimentally-determined surface field values, was difficult to ascertain from the experimental setup* and that an average value was used for the relative permittivity of rexolite. The theoretical curves, nonetheless, do exhibit the correct shape for the surface electric field, i.e., a monotonically-increasing amplitude which peaks and then falls as the tip is approached.

_____

*Unfortunately, the experimental setup has been dismantled, which prevented duplicating the measurements to further substantiate their validity.

6. CONCLUSION

A theory has evolved which appears to yield an approximate solution for the surface field on a dielectric wedge. The surface field exhibits meaningful physical characteristics such as magnitude which peaks and a phase variation which predicts launching. The analysis is very general and can be adapted with relative ease to a variety of two-dimensional tapers such as wedges with curved boundaries. In addition, certain three-dimensional geometries such as cones or pyramidal-type structures might be amenable to such analysis.

7. ACKNOWLEDGEMENT

8. REFERENCES

1. Levin, B.J. and Kietzer, J.E. "Hybrid Millimeter-Wave Integrated Circuits" Tech. Rept. ECOM-74-0577-F, Contract DAAB07-74-C-0577, performed for the U.S. Army Electronic Command, Fort Monmouth, N.J. by ITT Research Institute, Chicago, Ill. October 1975.

2. Andersen, J. Bach, "Metallic and Dielectric Antennas," Copenhagen: Polyteknisk Forlav, 1971.

3. James, J.R. "Engineering Approach to the Design of Tapered Dielectric-rod and Horn Antennas," Radio and Electronic Engineer, Vol. 42, No. 6, June 1972.

4. Tien, P.K., Smolinsky, G., and Martin, R.J., "Radiation Fields of a Tapered Film and a Novel Film-to-Fiber Coupler," IEEE Trans. Microwave Theory and Techniques, Vol. MTT-23, No. 1, Jan 1973.

5. Bates, R.H.T., "Wave Functions for Prisms," Int. J. Electronics, Vol. 34, No. 1, 1973.

6. Balling, P., "Radiation from the Dielectric Wedge," Licentiate Thesis LD20, Lab. Electromagn. Theory, Tech. Univ. Denmark, Lyngby, Denmark, 1971.

7. Balling, P. "Surface Fields on the Source-Excited Dielectric Wedge," IEEE Trans. Antennas Propagat. (Commun.), Vol. AP-21, Jan. 1973.

8. Marcuse, D., "Radiation Losses of Tapered Dielectric Slab Waveguides," Bell System Tech. Journal, Feb. 1970.

9. Marcuse, D. "Theory of Dielectric Optical Waveguides," Academic Press, N.Y. 1974.

10. Kumar, A. and Chatterjee, R., "Radiation from Tapered Dielectric Rod Aerials," J. Indian Inst. Sci., Vol. 51, Oct. 1968

11. Schwering, F., Private Communication, U.S. Army Communications Research and Development Command, Fort Monmouth, N.J.

12. Shevchenko, V.V., "Continuous Transitions in Open Waveguides," Golem Press, 1971.

13. Bahar, E., "Propagation of Radio Waves over a Non-Uniform Layered Medium," Radio Science, Vol. 5, July 1970.

14. Balling, P., "On the Role of Lateral Waves in the Radiation from the Dielectric Wedge," IEEE Trans. Antennas Propagat. (Commun.) Vol. AP-21, March 1973.

15. Felsen, L.B. and Maurer, S.J., "Ray Interpretation of Modes in Curved Nonuniform Waveguides," Electronic Letters, Vol. 4, No. 4, Feb. 1968.

16. Maurer, S.J. and Felsen, L.B., "Ray Optical Techniques for Guided Waves," Proc. of IEEE, Vol. 55, No. 10, Oct. 1967.

17. Maurer, S.J. and Felsen, L.B., "Ray Methods for Trapped and Slightly Leaky Modes in Multilayered and Multiwave Regions," IEEE Trans. on MTT, Sept. 1970, pp. 584-594.

18. Maurer, S.J. and Felsen, L.B., "Ray-Optical Methods for Modes in Guiding and Radiation Structures," Polytechnic Institute of Brooklyn, Report PIBEP-68-004, June 1968.

19. Maurer, S.J. and Siwiak, K., "Quasi-Optic Methods for Near Field Determination on a Dielectric Wedge," URSI Conference, Washington, D.C., Spring, 1972.

20. Siwiak, K., "A Dielectric Wedge Analysis by Ray Optics," Masters Thesis, Advisor: Maurer, S.J., Polytechnic Inst. of New York, June 1972.

21. Gopen, C. W., "Near Field for a Dielectric Wedge by Ray Methods," Masters Thesis, Advisor: Maurer, S.J., Polytechnic Inst. of New York, June 1971.

22. Marcuse, D., "Light Transmission Optics," Van Nostrand Reinhold Co., New York, 1972.

23. Seshadri, S.R., "Fundamentals of Transmission Lines and Electromagnetic Fields," Addison-Wesley Publishing Co., Mass., 1971.

24. Whitman, G., and Maurer, S.J., "Integrated Dielectric Resonator and Antenna Millimeter-Wave Structures," Tech. Report NJIT 10, New Jersey Inst. of Tech., Oct. 1975.

25. Felsen, L.B. and Marcuvitz, N., Radiation and Scattering of Waves, Prentice-Hall, New Jersey, 1973.

26. Sommerfeld, A., Partial Differential Equations in Physics, New York: Academic Press, Inc., 1949.

27. Levey, L. and Maurer, S.J., "Uniform Asymptotic Representation of Beam Modes," Journal of the Optical Society, Vol. 61, No. 12, Dec. 1971.

APPENDIX A. RAY OPTICS

The ray optical solution to the reduced wave equation

$$(\nabla^2 + k^2) \, u(\underline{r}) = 0 \qquad\qquad\qquad (A1)$$

is sought. The quantity $k = \omega \sqrt{\mu_o \epsilon_o \epsilon_r}$ denotes the wavenumber of a homogeneous lossless dielectric of relative dielectric constant ϵ_r. A time dependence of exp $(-i\omega t)$ is assumed and suppressed. To obtain a unique solution of (A1), either the tangential electric and magnetic fields at the air-dielectric surfaces must be continuous or the tangent electric field on the boundary must be linearly related to the tangent magnetic field (the so-called "impedance boundary condition") which can be expressed by the relation

$$-ik \, u(\underline{r}) + \frac{Z_s(\underline{r})}{\eta} \frac{\partial u(\underline{r})}{\partial \nu} = 0 \qquad \text{on B} \qquad\qquad (A2)$$

where ν is the outward normal to the boundary surface B, η is the intrinsic impedance of the dielectric, $Z_s(\underline{r})$ is a surface impedance, and $u(\underline{r})$ represents the transverse electric field component E_z.

Following the development by Maurer and Felsen [16], a geometric optics solution for large k of the form

$$u(\underline{r}) \sim \sum_{p=1}^{N} A_p(\underline{r}) \, e^{ikS_p(\underline{r})} \qquad\qquad\qquad (A3)$$

is assumed. Each species (denoted by p) has an amplitude $A_p(\underline{r})$ and a normalized phase $S_p(\underline{r})$. Inserting (A3) into (A1) and equating to zero,

the coefficients of the k^2 and of the k terms give, respectively,

$$(\nabla S_p(\underline{r}))^2 = 1 \qquad (A4)$$

and

$$2 \nabla S_p(\underline{r}) \cdot \nabla A_p(\underline{r}) + A_p(\underline{r}) \nabla^2 S_p(\underline{r}) = 0 \qquad (A5)$$

for any species p. Eqs. (A4) and (A5) are, respectively, the eiconal and transport equations of geometrical optics. Their solutions provide amplitude and phase variations of the rays. It should be emphasized that ray solutions are only asymptotic expressions and are not full wave solutions. One way of explaining the accuracy of a ray solution is to compare it with the asymptotic form of a full wave solution.

Substituting the ray solution (A5) into the boundary condition (A2) yields

$$\sum_{p=1}^{N} e^{ik S_p(\underline{r})} A_p(\underline{r}) \quad [- 1 + Z_s(\underline{r}) \frac{\partial S_p(\underline{r})}{\partial \nu}] = 0 \qquad (A6)$$

Eq. (A6) can be satisfied by postulating the pairwise vanishing of terms so that

$$e^{ik S_p} [A_p] \left[Z_s(\underline{r}) \frac{\partial S_p}{\partial \nu} - 1 \right] + e^{ik S_q} [A_q] \left[Z_s(\underline{r}) \frac{\partial S_q}{\partial \nu} - 1 \right] = 0$$
$$\text{on B} \qquad (A7)$$

Equating phases of the exponential terms in (A7) yields

$$k S_p = k S_q + 2\Pi m \qquad \text{on B,} \qquad (A8)$$

-37-

where m is an integer such that initially $\frac{2m\Pi}{k}$ is of order 1. From the eiconal equation (A4) and boundary condition (A8), it can be shown that

$$\frac{\partial S_p}{\partial \nu} = -\frac{\partial S_p}{\partial \nu} \qquad \text{on B} \tag{A9}$$

The minus sign enters into the above equation because reflection takes place at the boundary. Using (A8) and (A9) in (A7) gives

$$A_q = \Gamma A_p \qquad \text{on B} \tag{A10a}$$

where

$$\Gamma = \frac{\overline{z}_s(\underline{r}) \dfrac{\partial S_p}{\partial \nu} - 1}{\overline{z}_s(\underline{r}) \dfrac{\partial S_p}{\partial \nu} + 1} \tag{A10b}$$

Γ is recognized as a reflection coefficient and $\overline{z}_s = Z_s/\eta$.

If the reflection coefficient is constant on the boundary B, it is possible to construct an alternative formation without destroying the specular reflection condition (A9). In this formulation, the phase of Γ is incorporated into the phase function S rather than being totally associated with amplitude terms as was done in (A10). Rewriting (A7) in the form

$$A_q e^{ik S_q} = A_p \Gamma e^{ik S_p} = A_p |\Gamma| e^{i\arg\Gamma + ik S_p}, \tag{A11}$$

with Γ defined by (A10b), leads naturally to the relations

$$A_q = A_p |\Gamma|, \quad k S_q = k S_p + \arg \Gamma - 2m\Pi. \tag{A12}$$

-38-

If, furthermore, $|\Gamma| = 1$, then $\arg \Gamma = -i \ln \Gamma$ and (A12) reduces to

$$A_p = A_q ,\qquad\qquad\qquad\qquad (A13a)$$

$$k\, S_p = k\, S_q + i \ln \Gamma + 2m\Pi \qquad\qquad\qquad (A13b)$$

where m is an integer.

A.   Surface Field

Two computer programs are used to compute the surface field for the wedge antenna. Since only the tangential components of the electromagnetic field are required to calculate the far field, only (3.34) and (3.35) are used. They are repeated here for convenience.

$$
E_z = - \sum_{n=1}^{N} \left\{ B_1 e^{-jka(\Pi-\beta)/2} \int_{w_T-(n-1)\beta}^{w_T-n\beta} e^{-jkr \sin w + j\,kaw} (1 + \Gamma(w)) \cdot \right.
$$

$$
\left. \cdot \prod_{m=1}^{n-1} \left(\frac{\Gamma(w + m\beta)}{\Gamma_T^{n-1}} \right) dw \right\} \tag{B1}
$$

$$
H_r = - \sum_{n=1}^{N} \left\{ \frac{B_1}{\eta} e^{-jka(\Pi-\beta)/2} \int_{w_T-(n-1)\beta}^{w_T-n\beta} e^{-jkr \sin w + j\,kaw} (1 - \Gamma(w)) \cdot \right.
$$

$$
\left. \cdot \prod_{m=1}^{n-1} \left(\frac{\Gamma(w + m\beta)}{\Gamma_T^{n-1}} \right) \cos w \, dw \right\} \tag{B2}
$$

Program 'One' evaluates the r-independent part of these two integrands, namely:

$$
(1 + \Gamma(w)) \prod_{m=1}^{n-1} \left(\frac{\Gamma(w + m\beta)}{\Gamma_T^{n-1}} \right) e^{-jkr \sin w} \tag{B3}
$$

and

$$(1 - \Gamma(w)) \prod_{m=1}^{n-1} \frac{\Gamma(w + m\beta)}{\Gamma_T^{n-1}} \ e^{-jkr \sin w} \cos w \qquad (B4)$$

as vector quantities and stores these vectors in a disc file as input data to program 'Two' to be integrated with the r-dependent parts of the program. This method is employed since calculating the product of reflection coefficients is very time-consuming and can be done once for each set of antenna parameters.

'One' requires as input: $k_o d$ the relative half width of the slab, $k_o \ell$ the relative length of the wedge, and ε_r the relative dielectric constant. Five values are calculated per β radians on the real w-axis, starting with w_T and ending when the magnitude of the product term is less than 10^{-5} since this is the only term affecting the magnitude of the integrand and has a maximum value equal to 2.

Program 'Two' computes the surface field for

$$\text{Integer} \ (\frac{kr_T}{2\pi}) \ * \ 8 + 1 \qquad (B5)$$

points on the wedge surface or 8 points per wavelength in the dielectric material.

'Two' reads the two vector quantities from the disc file created by 'One' and multiplies each vector by the appropriate function of r and w:

$$e^{-jkr \sin w} \qquad (B6a)$$

$$\frac{e^{-jkr \sin w}}{\eta} \qquad (B6b)$$

The trapezoidal rule is used to evaluate the integral. The two tangential

-41-

surface fields are in a disc file as input to program 'Farfld.'

Program 'Farfld' reads the two tangential surface fields from 'Two' and integrates these vectors in (4.9) using Romberg's method of integration. This requires integrating the surface field using first two points per dielectric wavelength, then four points per dielectric wavelength, and finally, eight points per dielectric wavelength. The far field is calculated for 5° increments from $0^o \leq \xi \leq 180^o$.

TABLE 1

Antenna Parameters

Identifying Letter	$k_o d$	$k_o \ell$	w_r	w_T	β	$k_o a$
A	1.54	14.65	2.56	65.57	12	6.03
B	1.54	49.00	2.56	65.57	3.6	20
C	1.54	95.49	2.56	65.57	1.85	39.4
D	2.0	95.49	2.56	69.7	2.4	33.08
E	1.0	95.49	2.56	58.47	1.2	49.86
F	1.0	95.49	3.24	59.49	1.2	48.4
G	1.0	95.49	2.0	58.49	1.2	49.83
H	0.5	10Π	12.0	56.49	1.824	17.34
I	0.5	20Π	12.0	56.49	0.912	34.69
J	1.53	48.69	2.56			
K	1.61	51.28	2.56			
L	1.67	15.92	2.56			
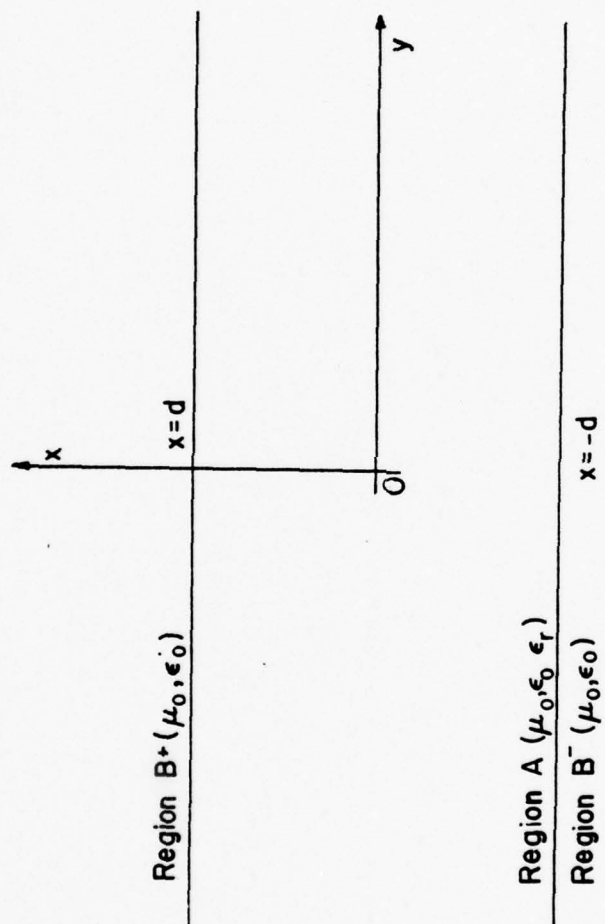
FIG. 1. Dielectric slab-coordinates and geometry.

Region B⁺ (μ_0, ϵ_0')

x

x=d

Region A $(\mu_0, \epsilon_0\, \epsilon_r)$

y

O

Region B⁻ (μ_0, ϵ_0)

x=-d

-44-
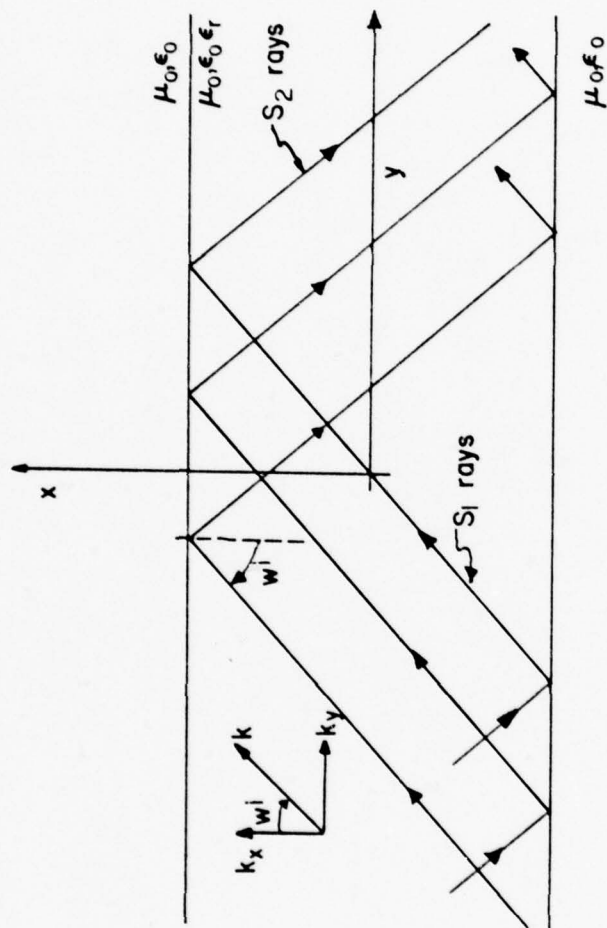
FIG. 2. Rays in the dielectric slab. Total internal reflection is assumed to occur at the air-dielectric interfaces.
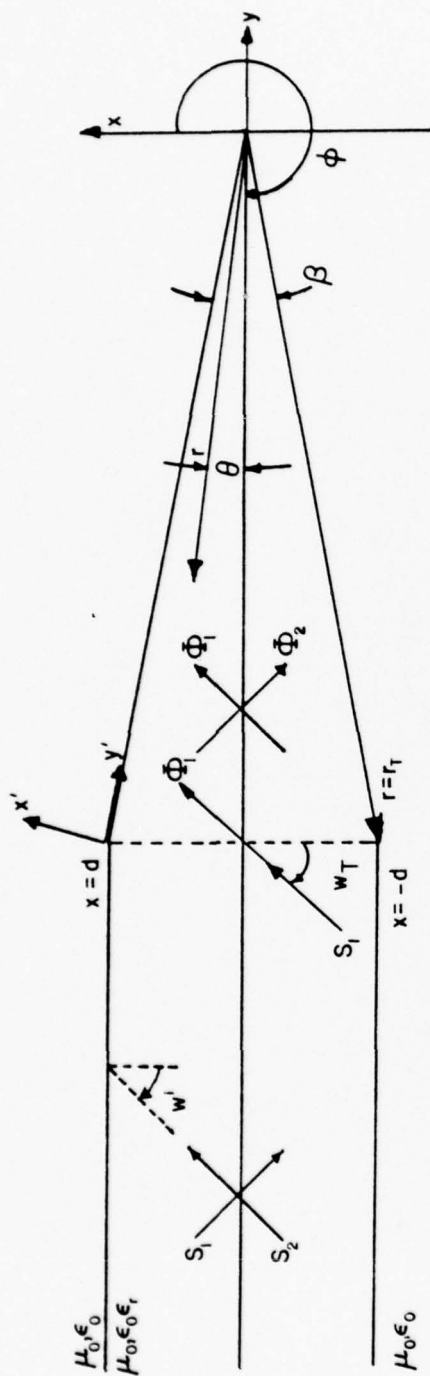
FIG. 3. Slab waveguide feeding the wedge antenna-coordinates and geometry.

$$\Phi_3 = a\theta + R(r) + C_3$$
$$\Phi_4 = -a\theta + R(r) + C_4$$

$$\Phi_1 = a\theta - R(r) + C_1, \quad R(r) = (r^2 - a^2)^{1/2} + a \cos^{-1}(a/r)$$
$$\Phi_2 = -a\theta - R(r) + C_2$$
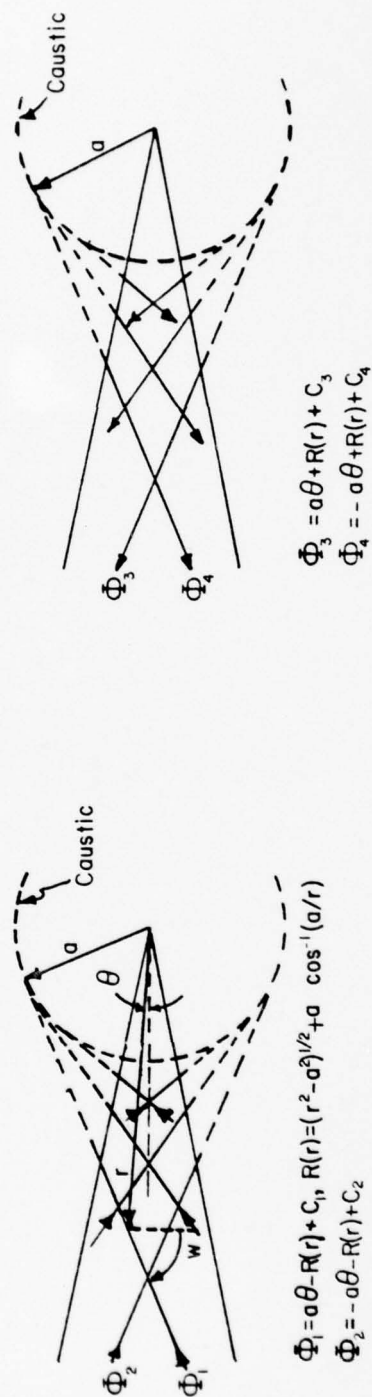
FIG. 4. Types of ray families in the wedge.

-46-
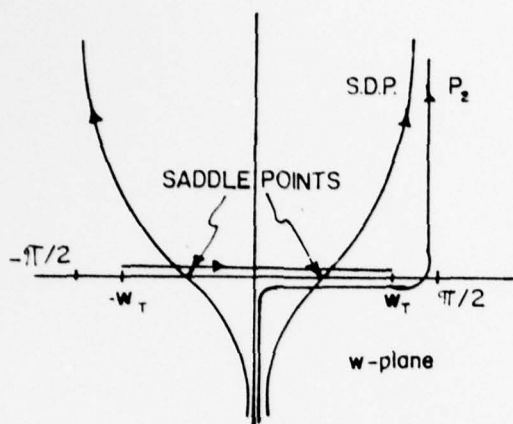
FIG. 5a. Integration paths in the
complex w-plane.
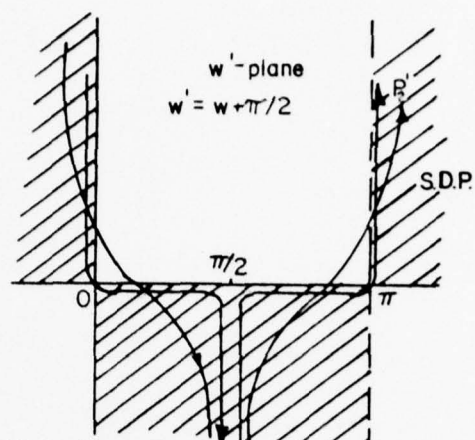
FIG. 5b. Integration paths for
Hankel function.
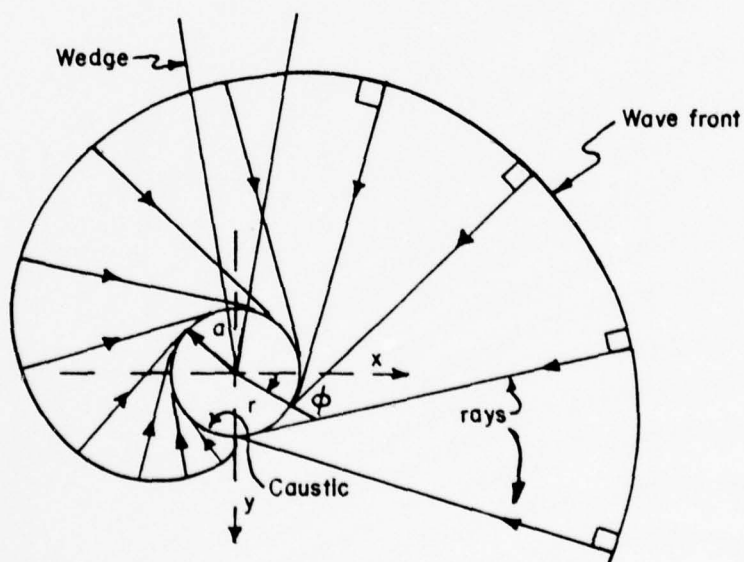
FIG. 6. Physical interpretation of $H_{ka}^{(2)}$ (kr) $e^{+jka\phi}$.
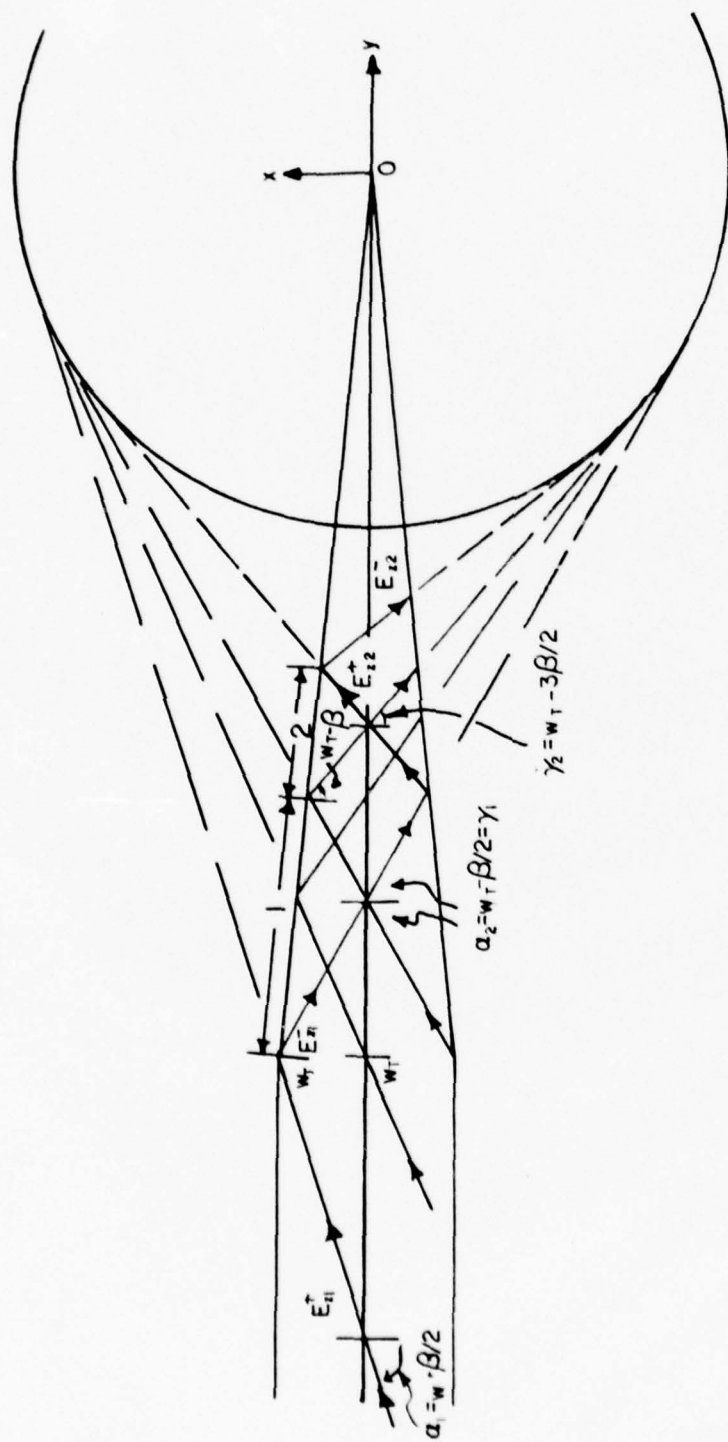
FIG. 7. Geometry for determining limits of integration on ray bundles.
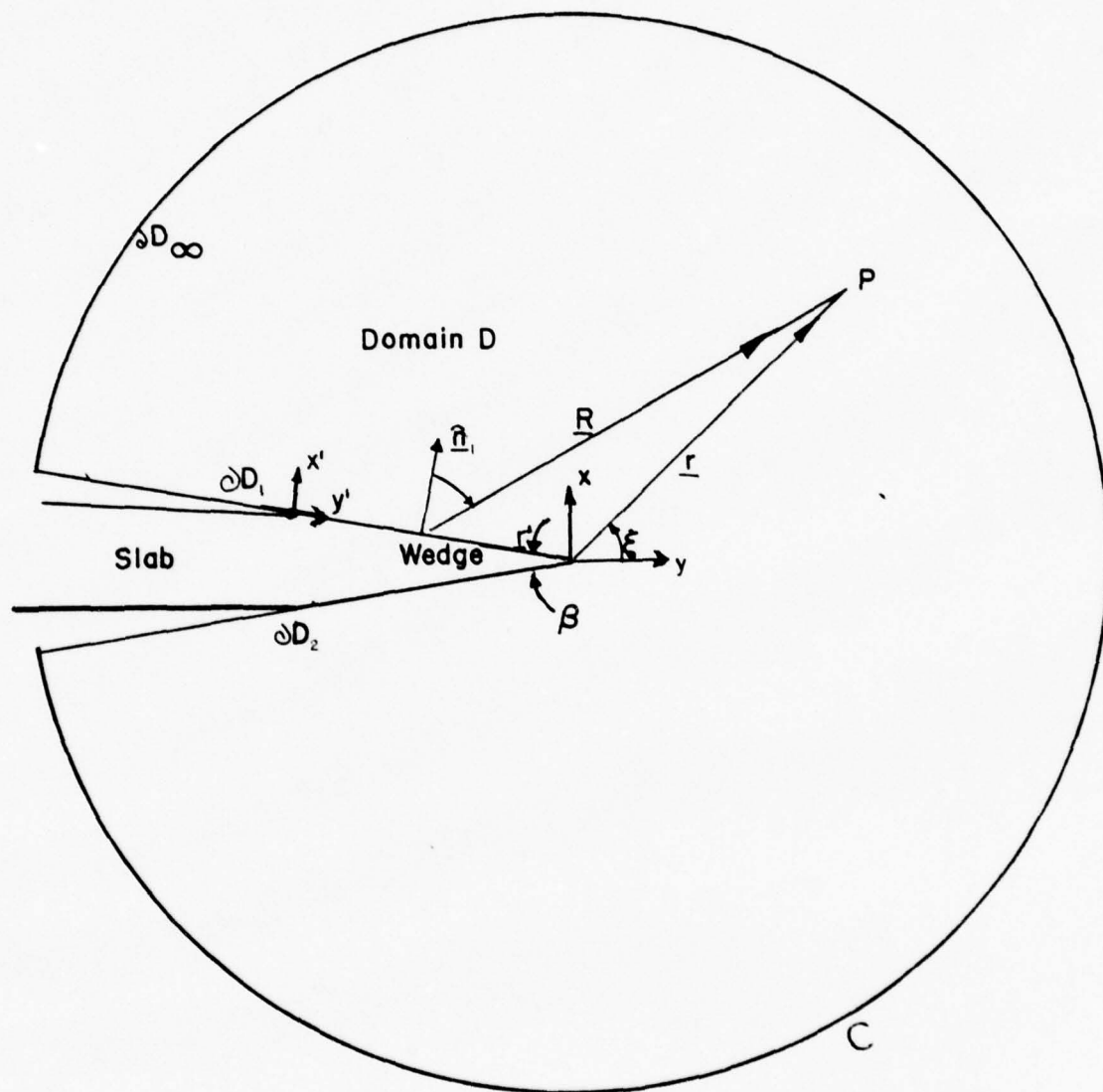
FIG. 8.   Geometry for calculating the far field.

-49-
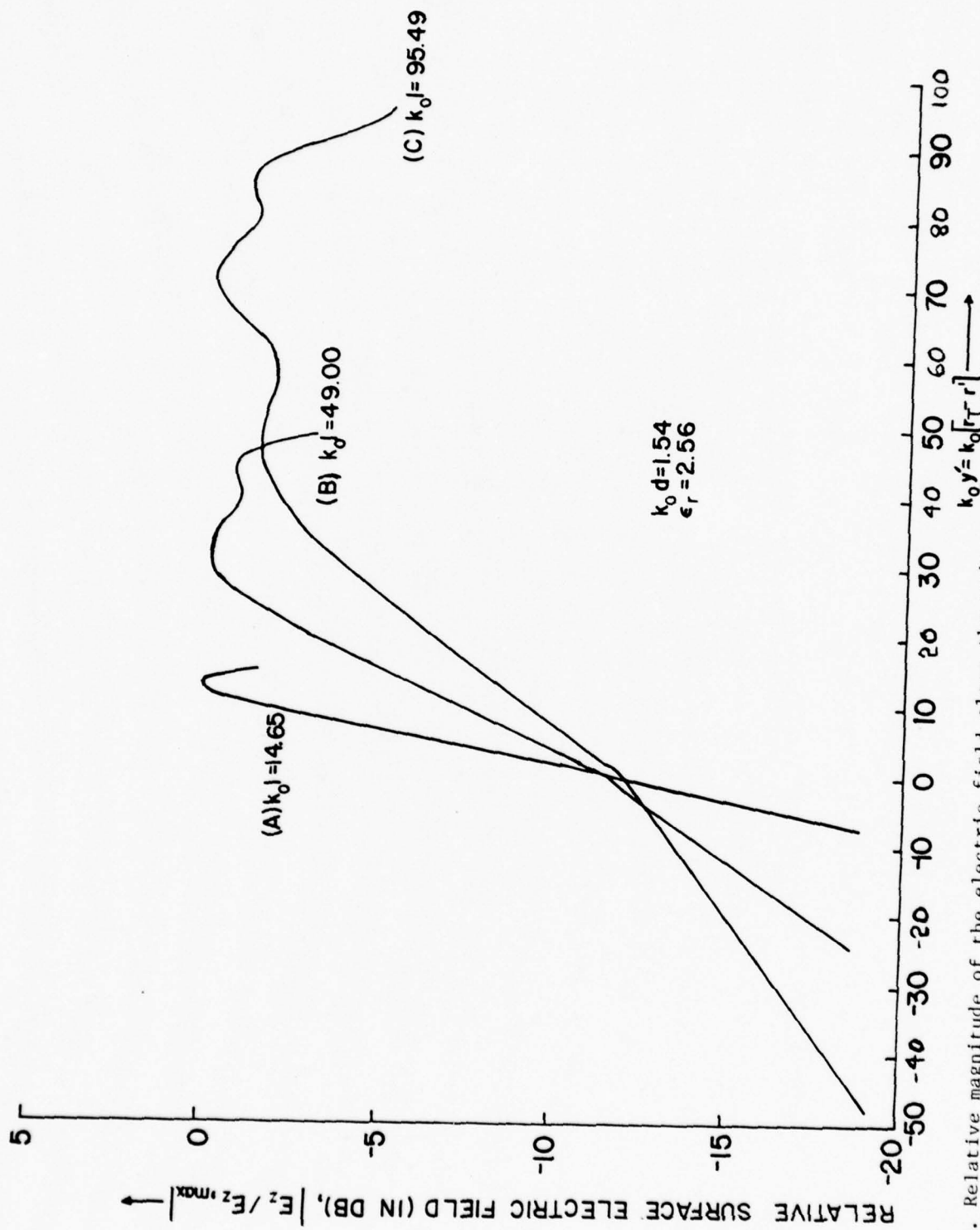
FIG. 9a. Relative magnitude of the electric field along the wedge surface and along its geometric extension into the evanescent region of the slab.
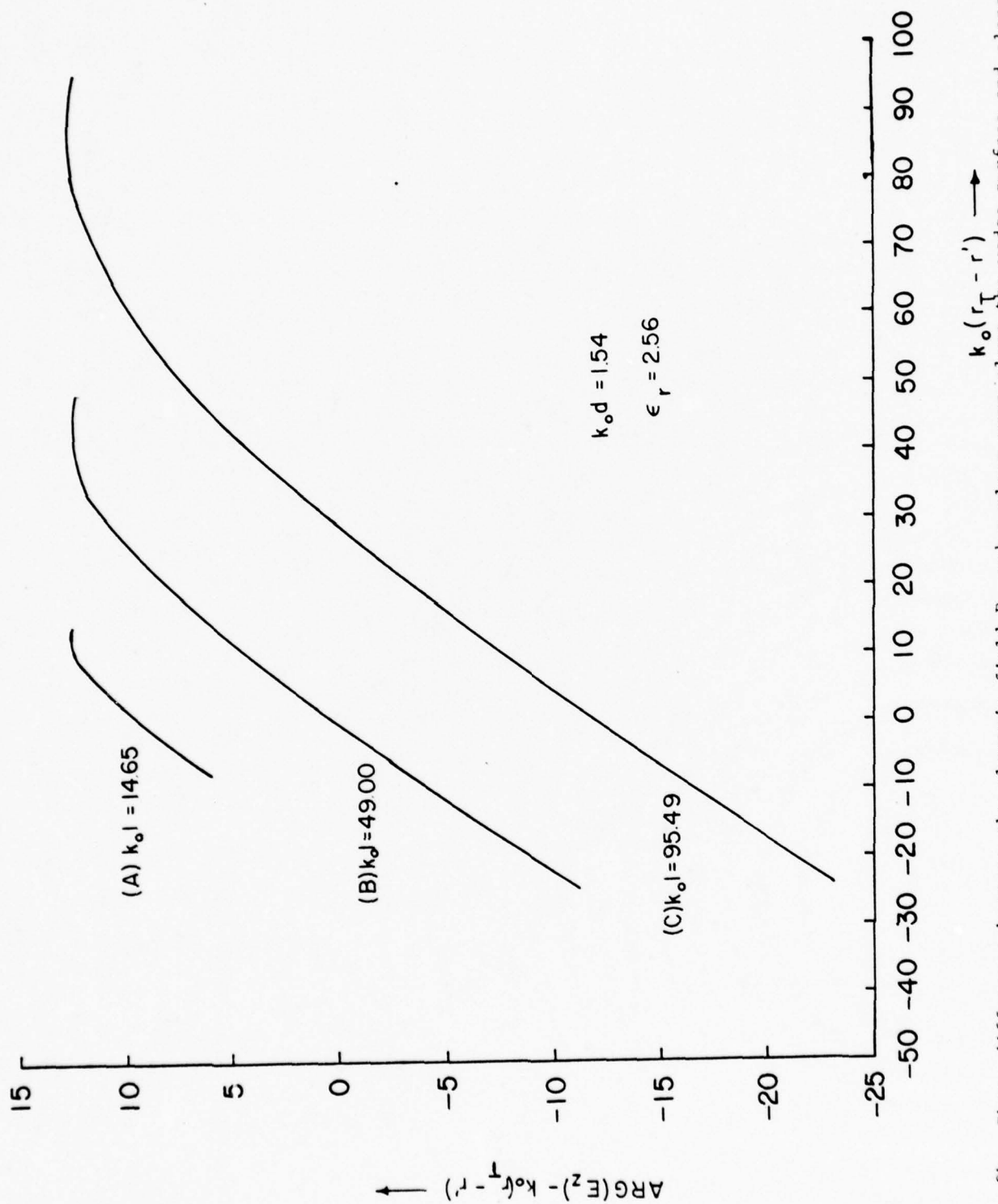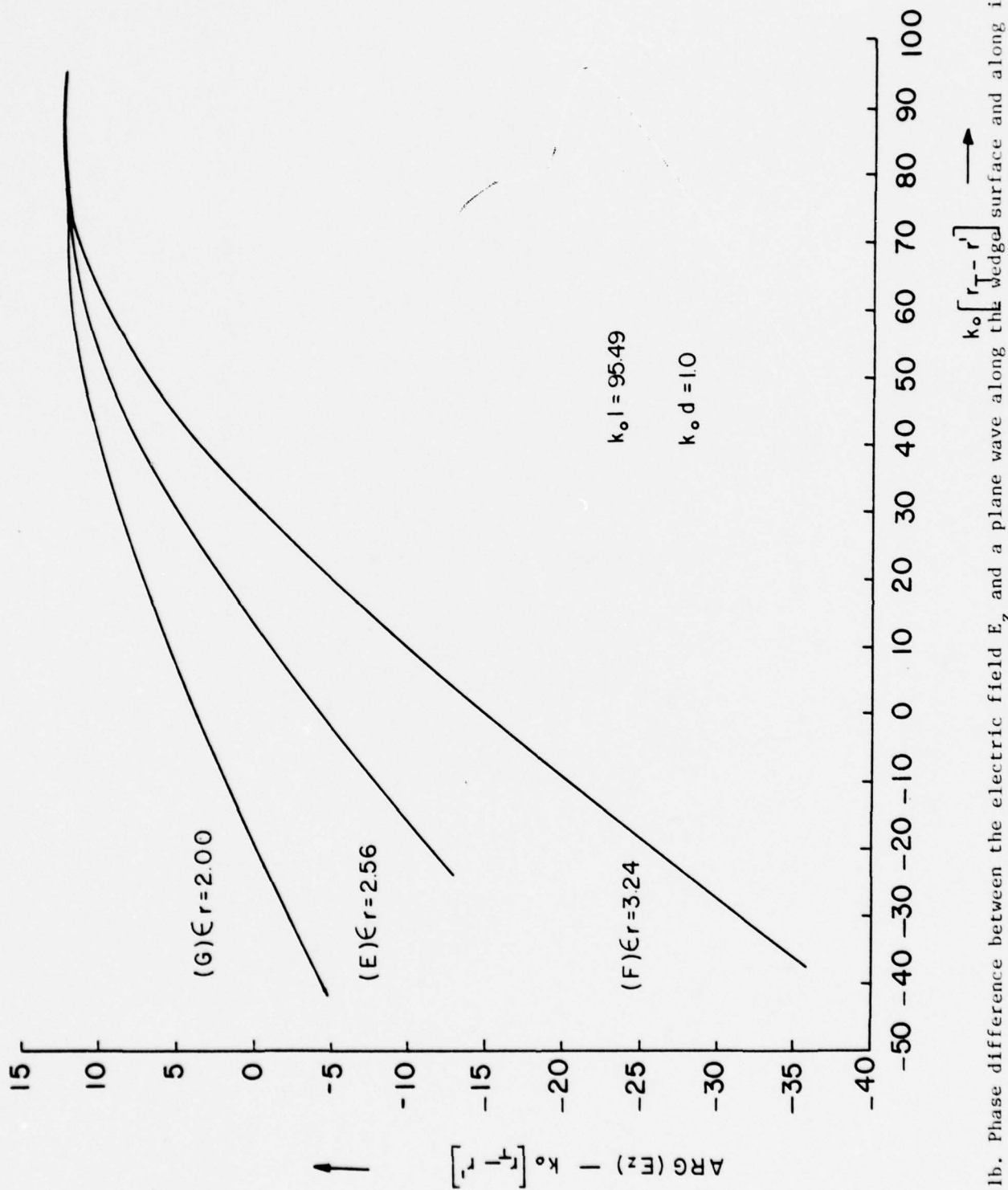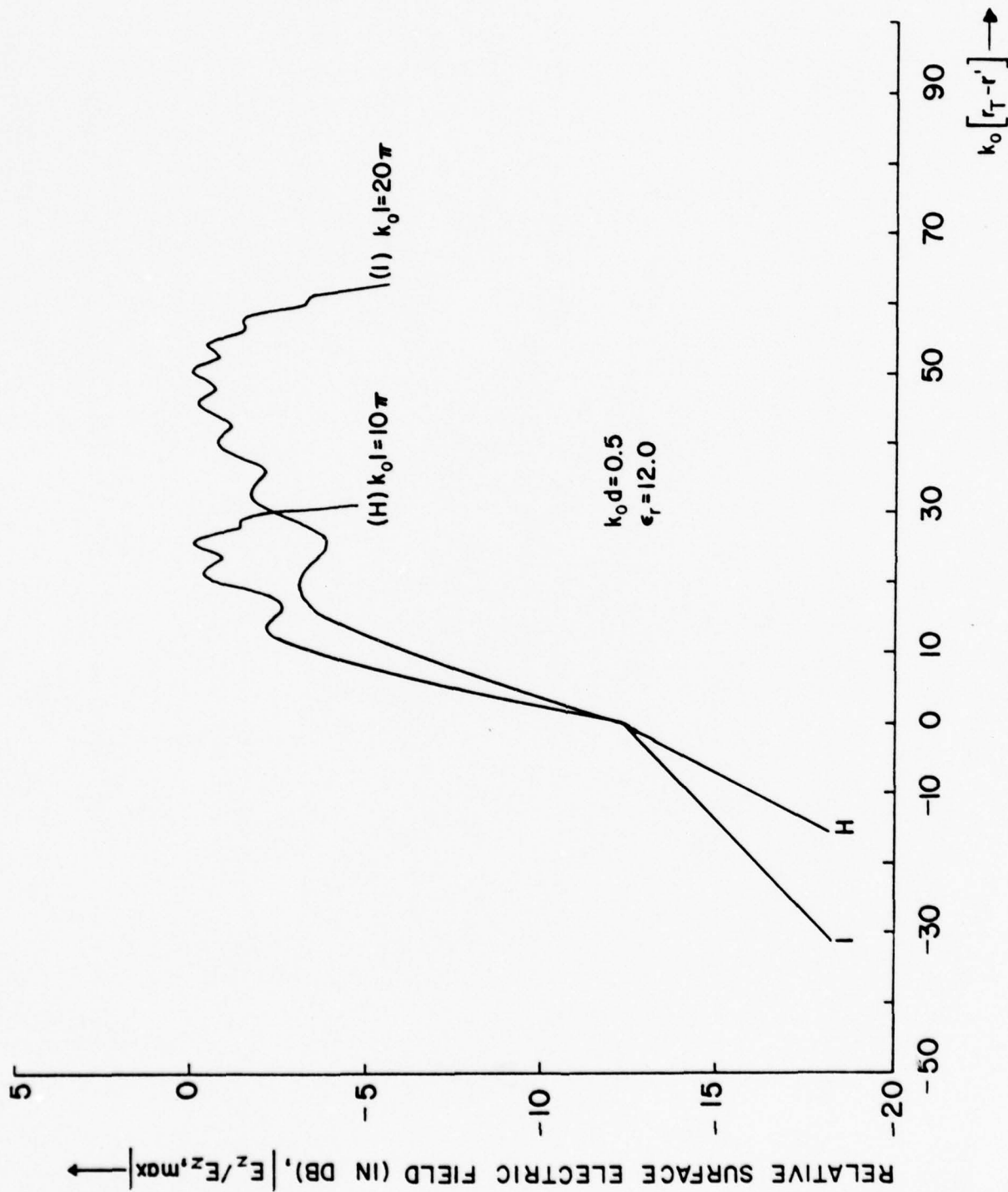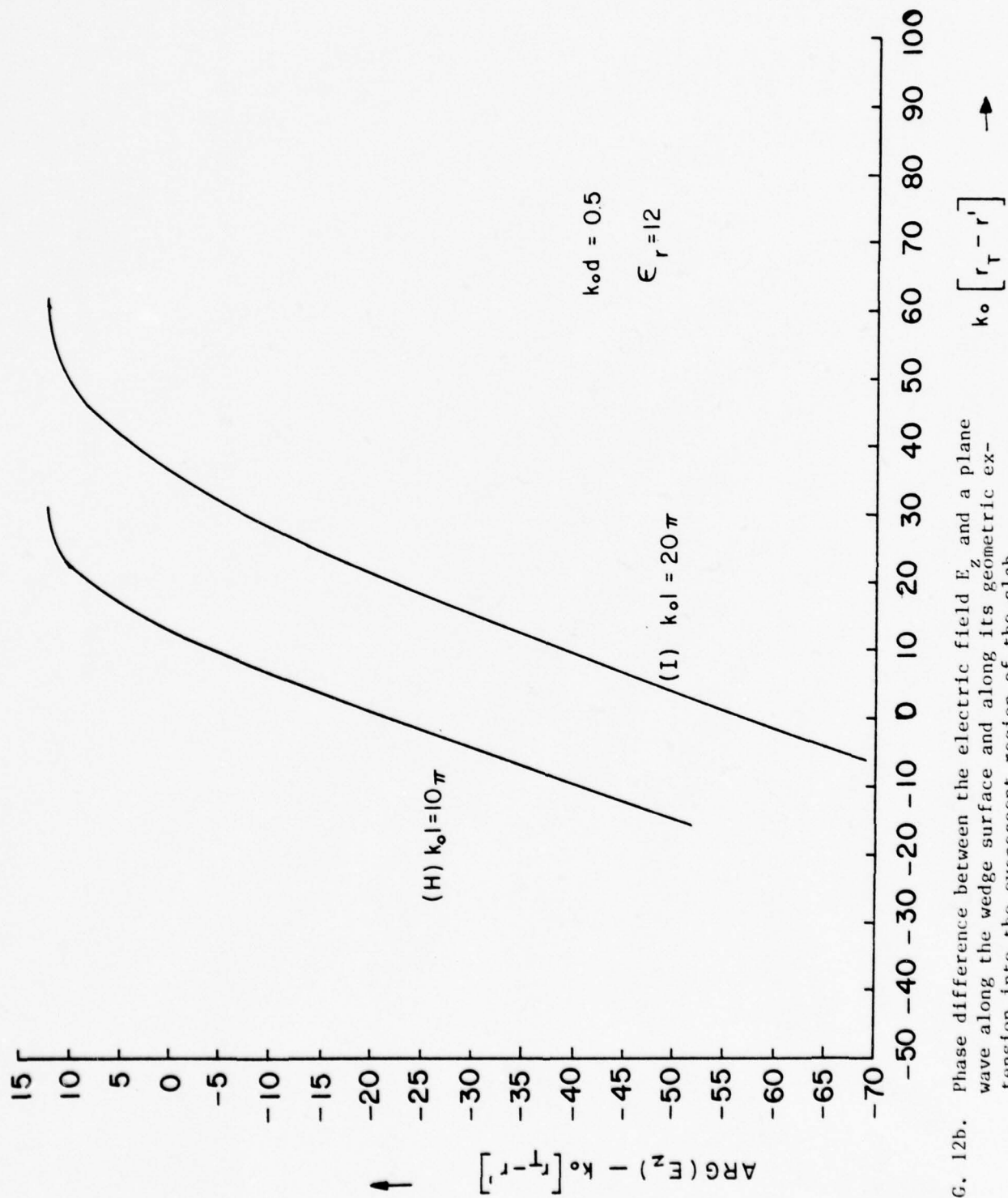
FIG. 9b. Phase difference between the electric field E_z and a plane wave along the wedge surface and along its geometric extension into the evanescent region of the slab.
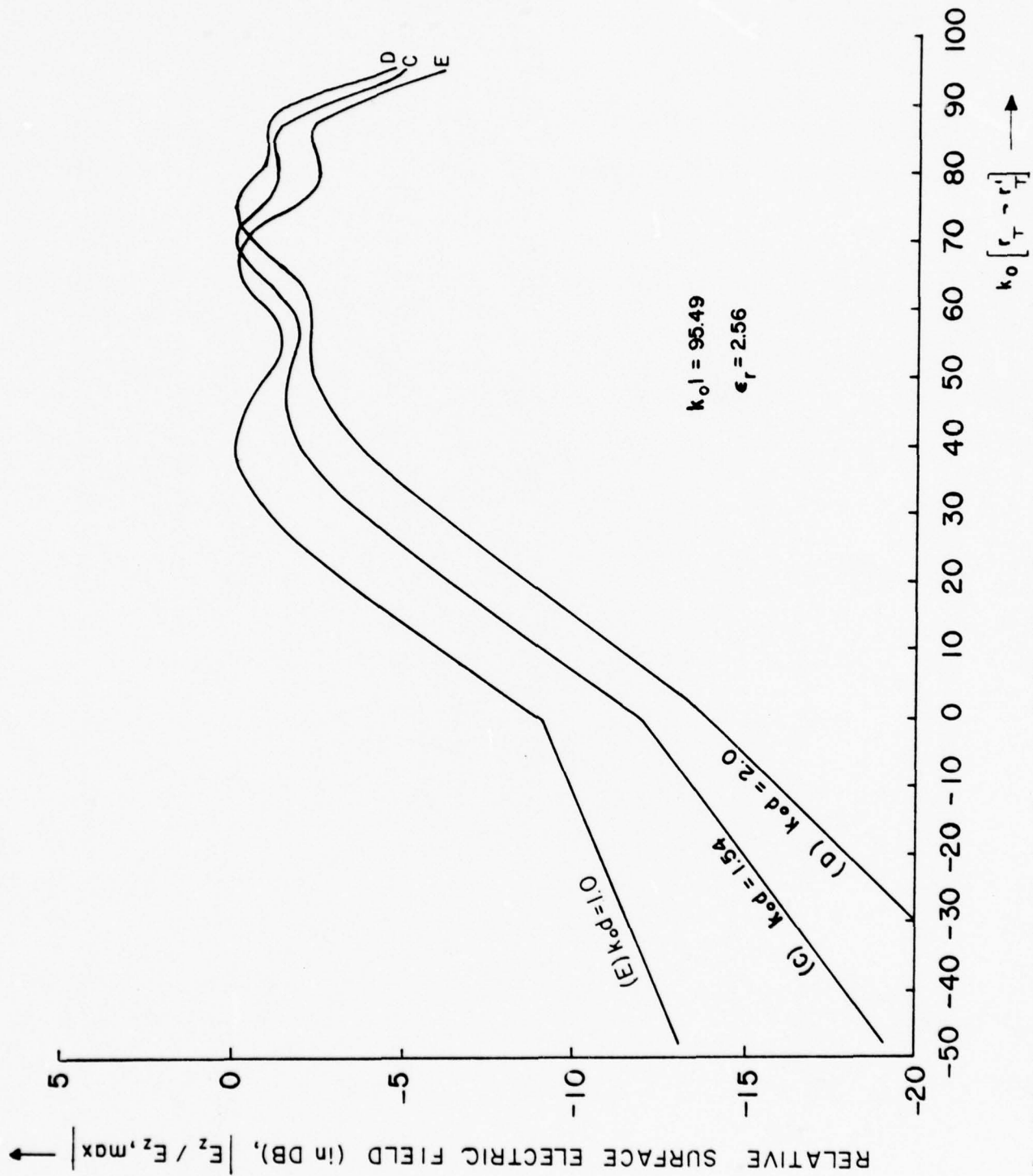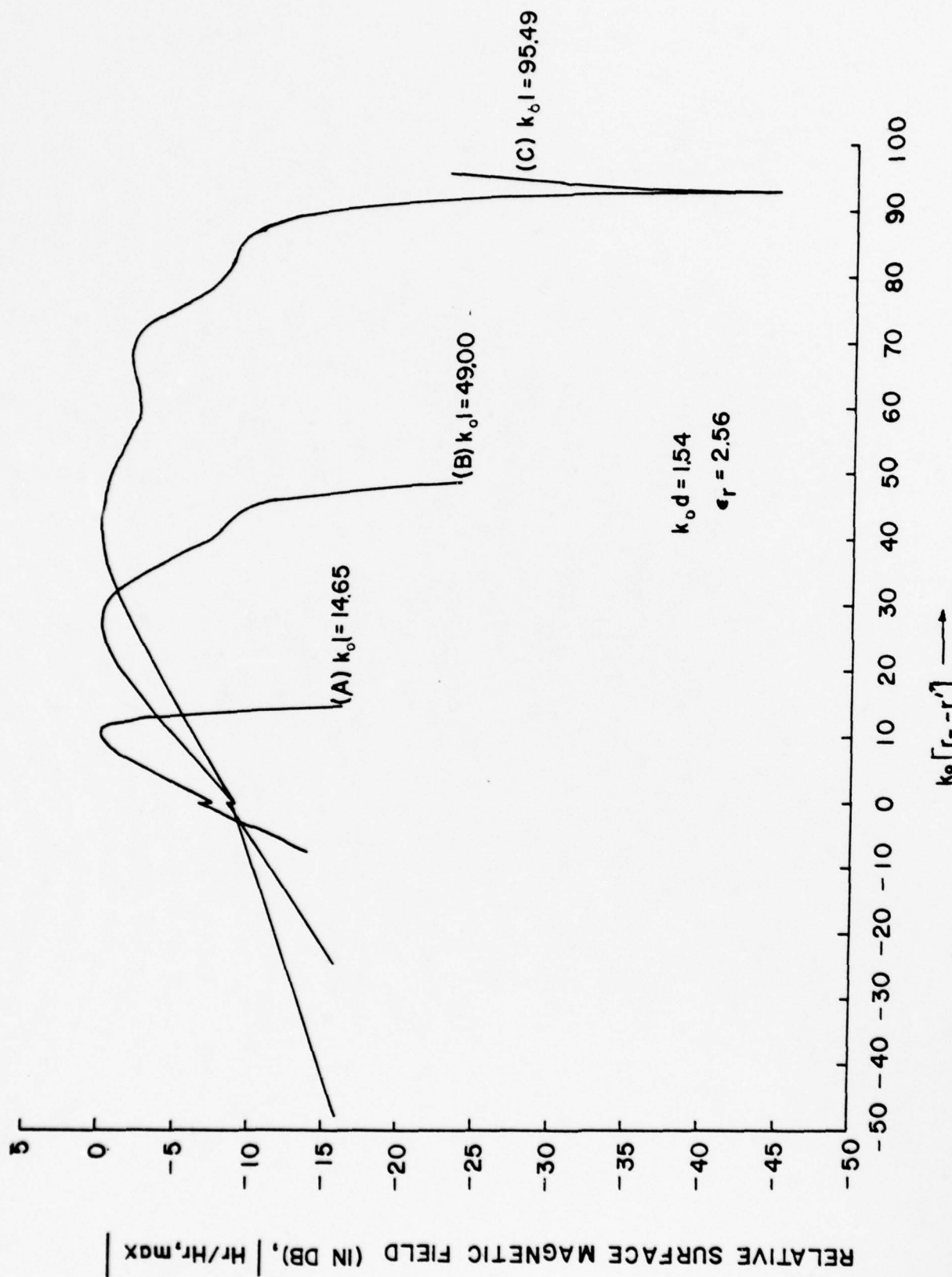
FIG. 10a. Relative magnitude of the electric field along the wedge surface and along its geometric extension into the evanescent region of the slab.

FIG. 10b. Phase difference between the electric field E_z and a plane wave along the wedge surface and along its geometric extension into the evanescent region of the slab.

$k_0 l = 95.49$

$\epsilon_r = 2.56$

(E) $k_0 d = 10$

(C) $k_0 d = 15.4$

(D) $k_0 d = 20$

$k_0 [r_T - r']$ →

← $ARG(E_z) - k_0 (r_T - r')$
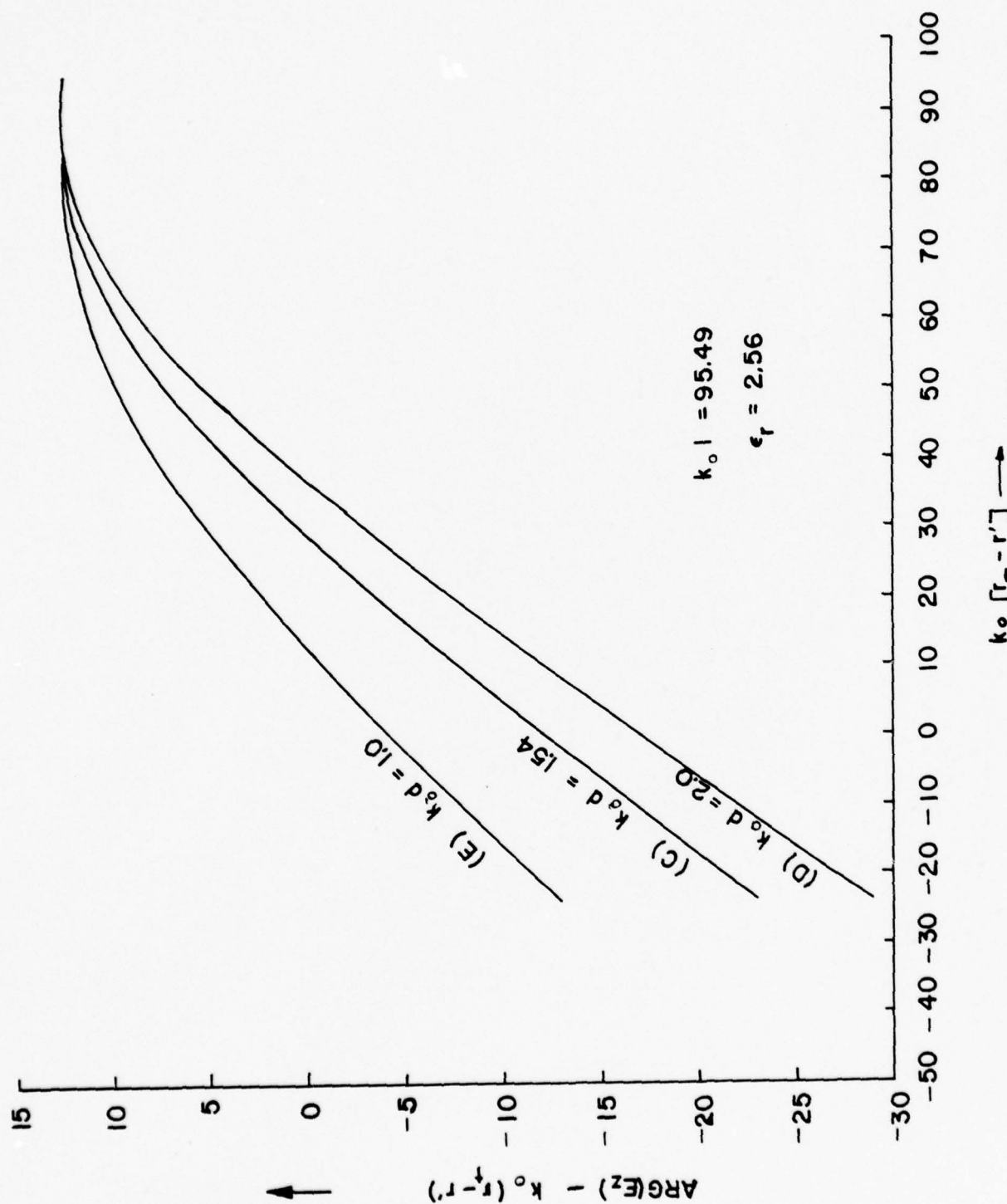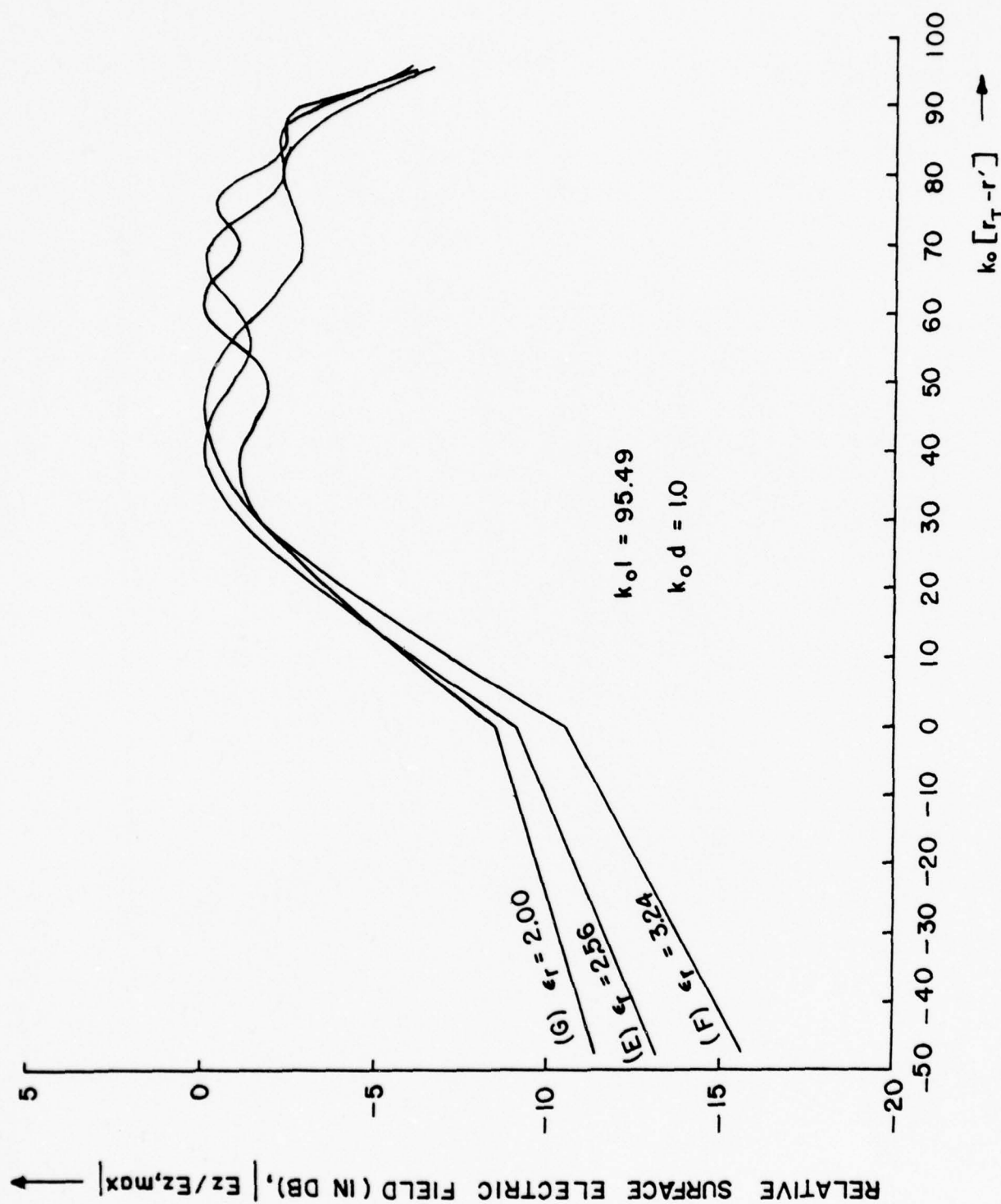
FIG. 11a. Relative magnitude of the electric field along the wedge surface and along its geometric extension into the evanescent region of the slab.
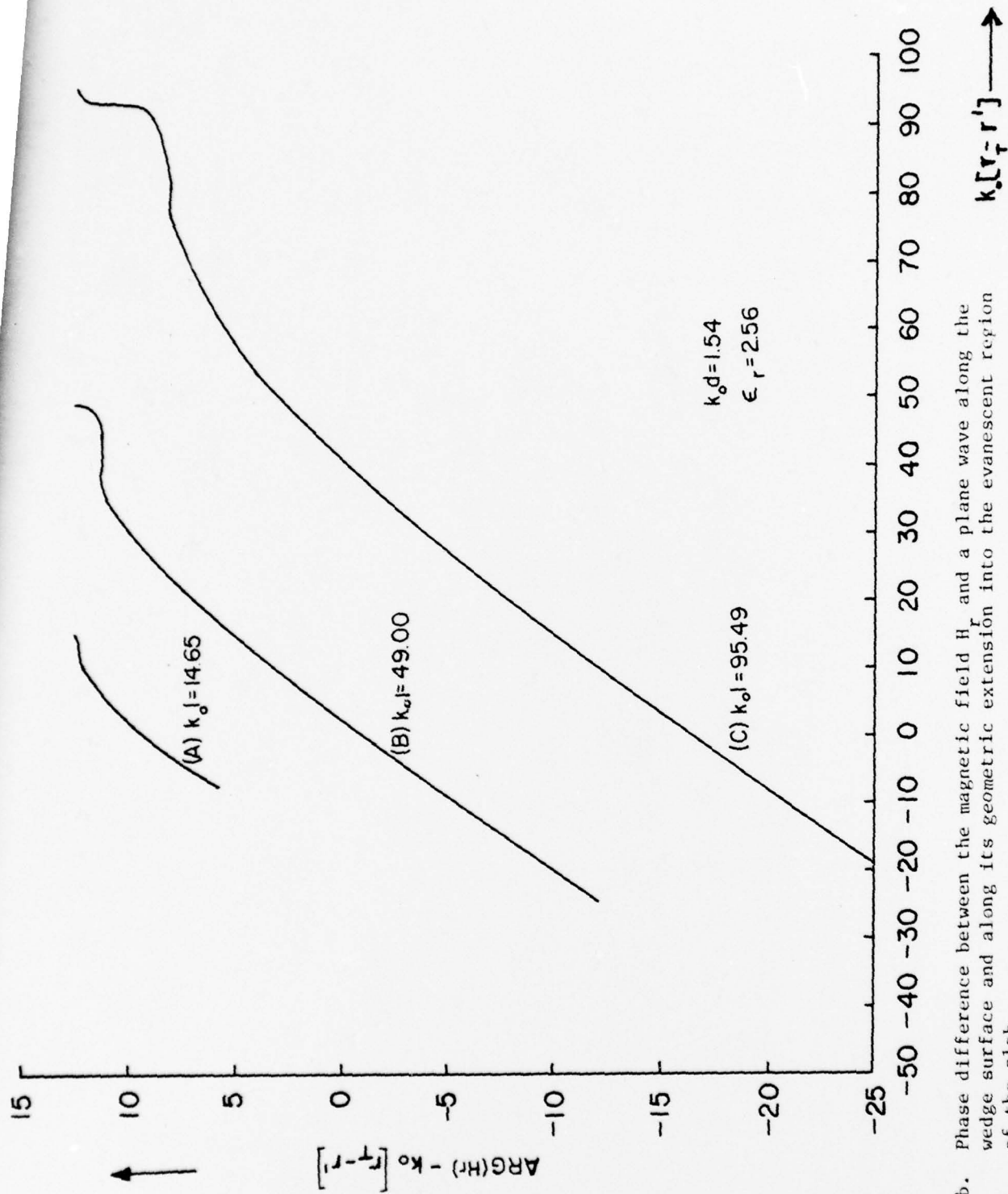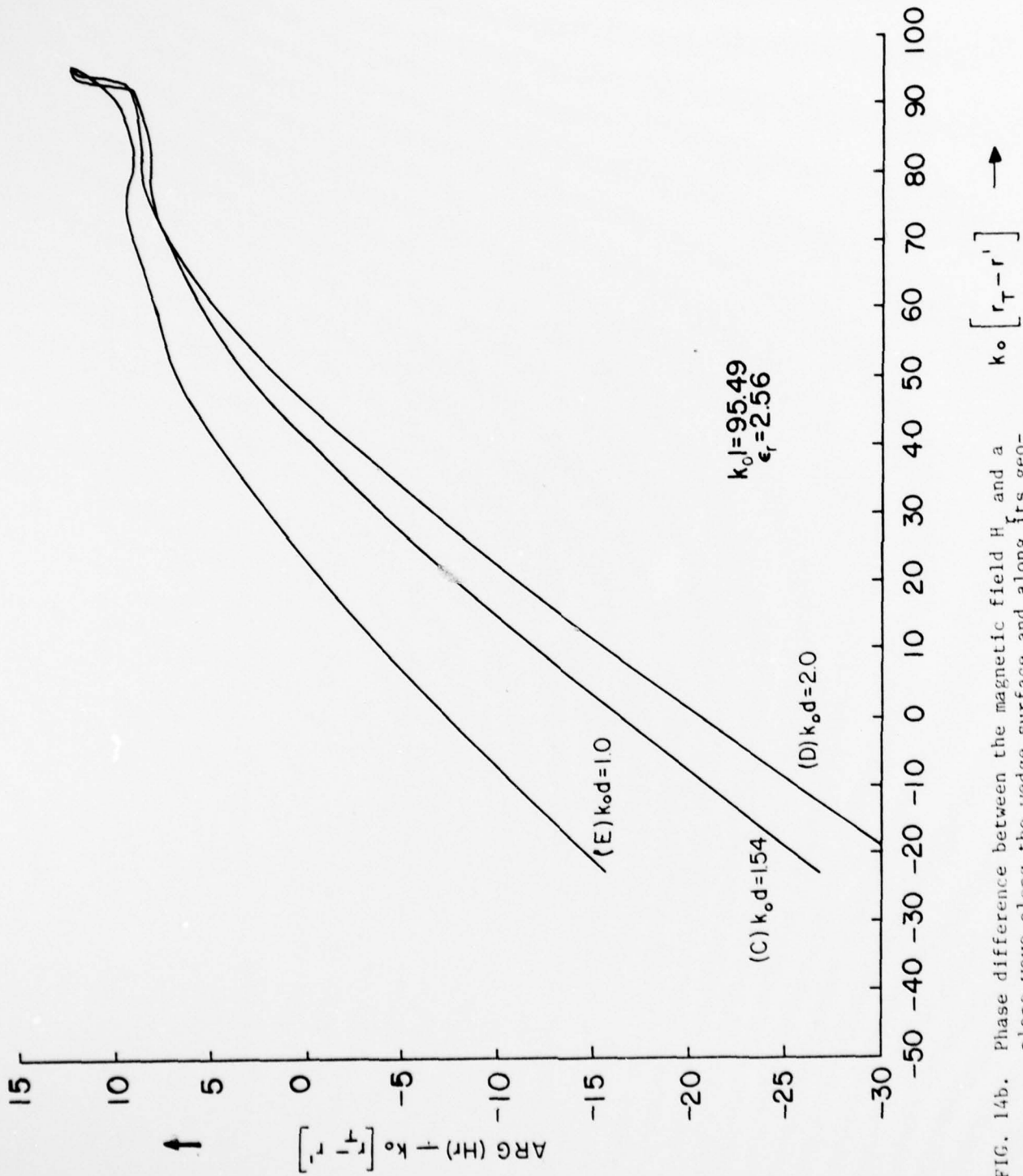
-54-

FIG. 11b. Phase difference between the electric field E_z and a plane wave along the wedge surface and along its geometric extension into the evanescent region of the slab.

FIG. 12a. Relative magnitude of the electric field along the wedge surface and along its geometric extension into the evanescent region of the slab.

FIG. 12b. Phase difference between the electric field E_z and a plane wave along the wedge surface and along its geometric extension into the evanescent region of the slab.
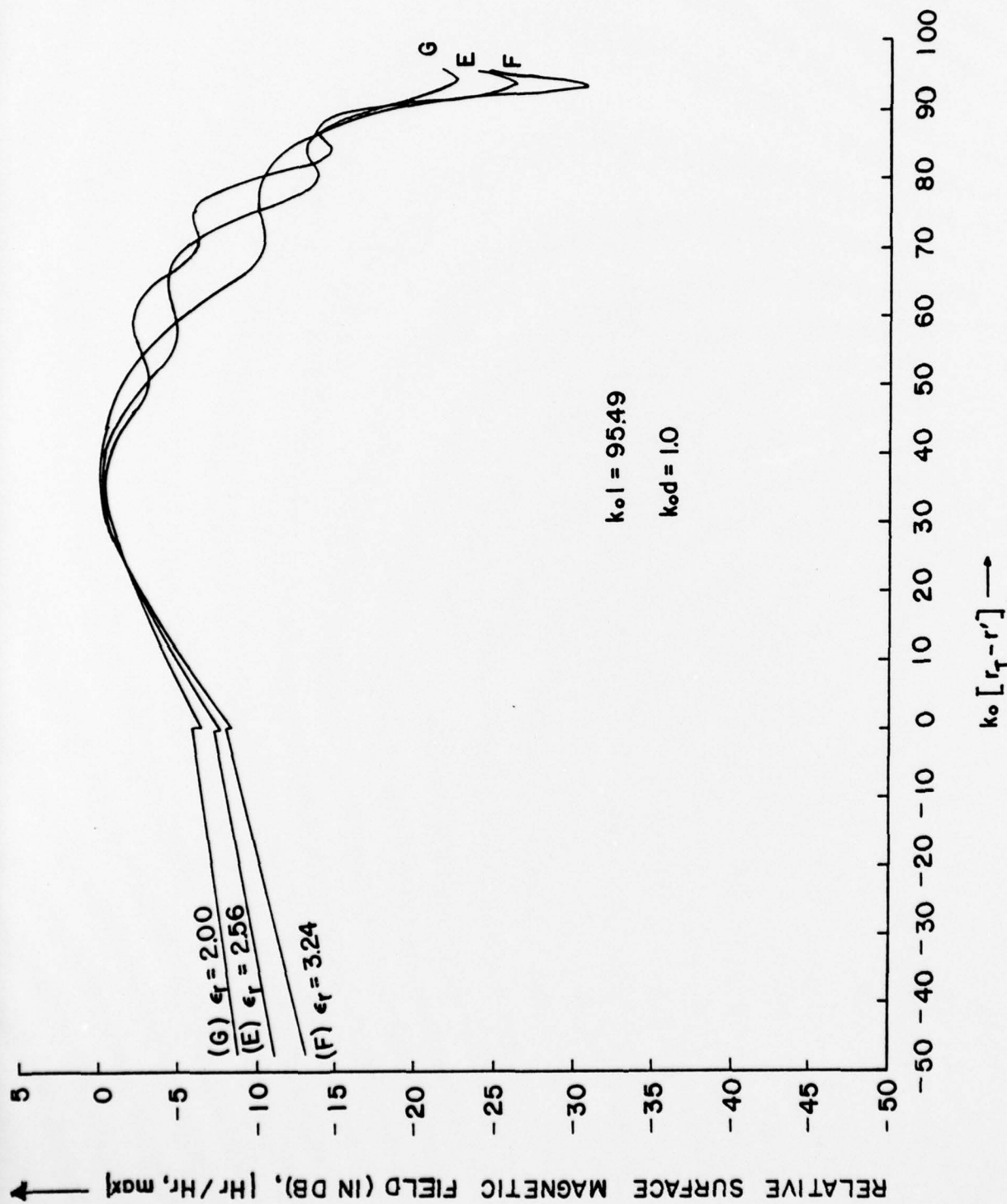
FIG. 13a. Relative magnitude of the tangential magnetic field along the wedge surface and along its geometric extension into the evanescent region of the slab.
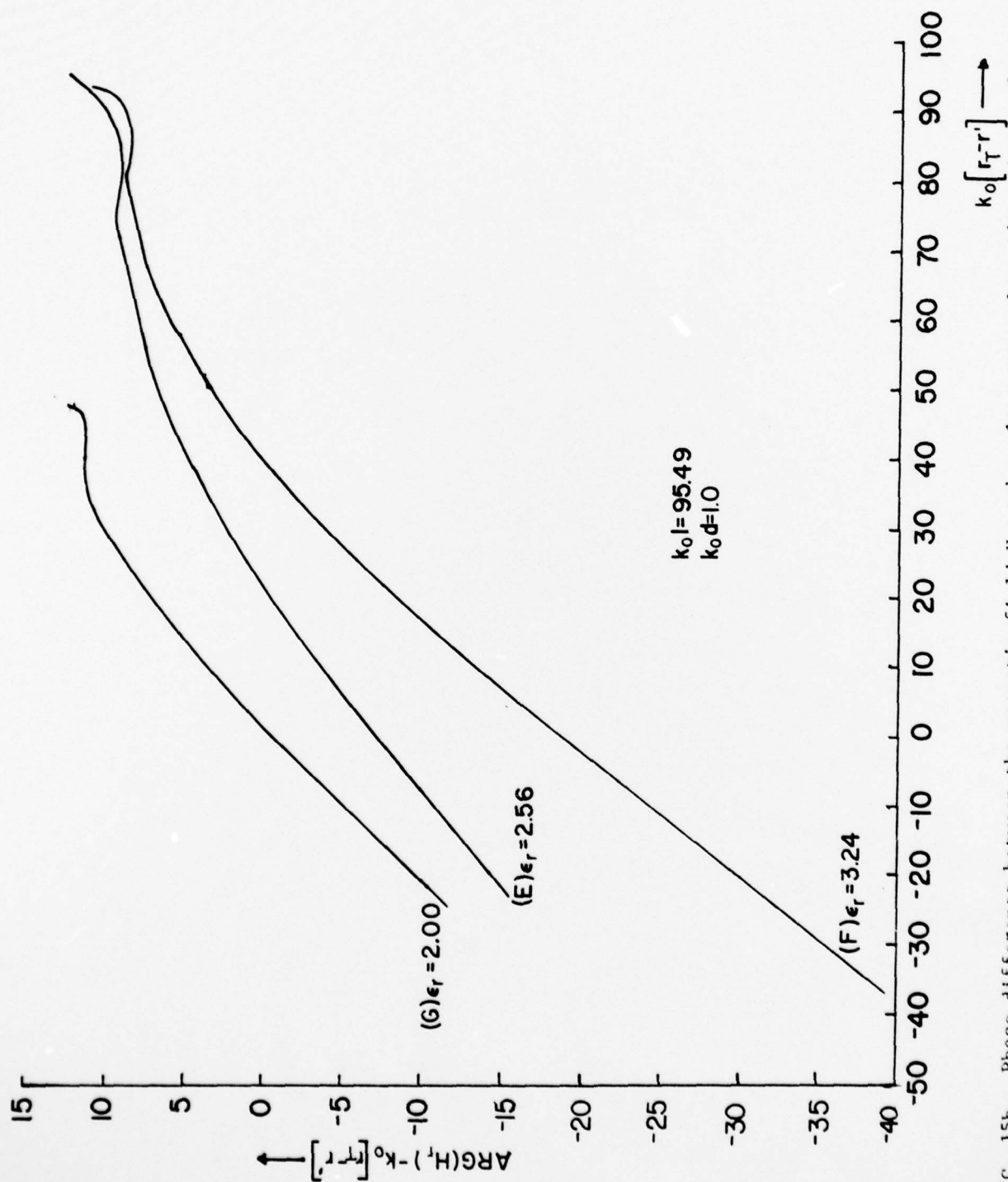
FIG. 13b. Phase difference between the magnetic field H_r and a plane wave along the wedge surface and along its geometric extension into the evanescent region of the slab.
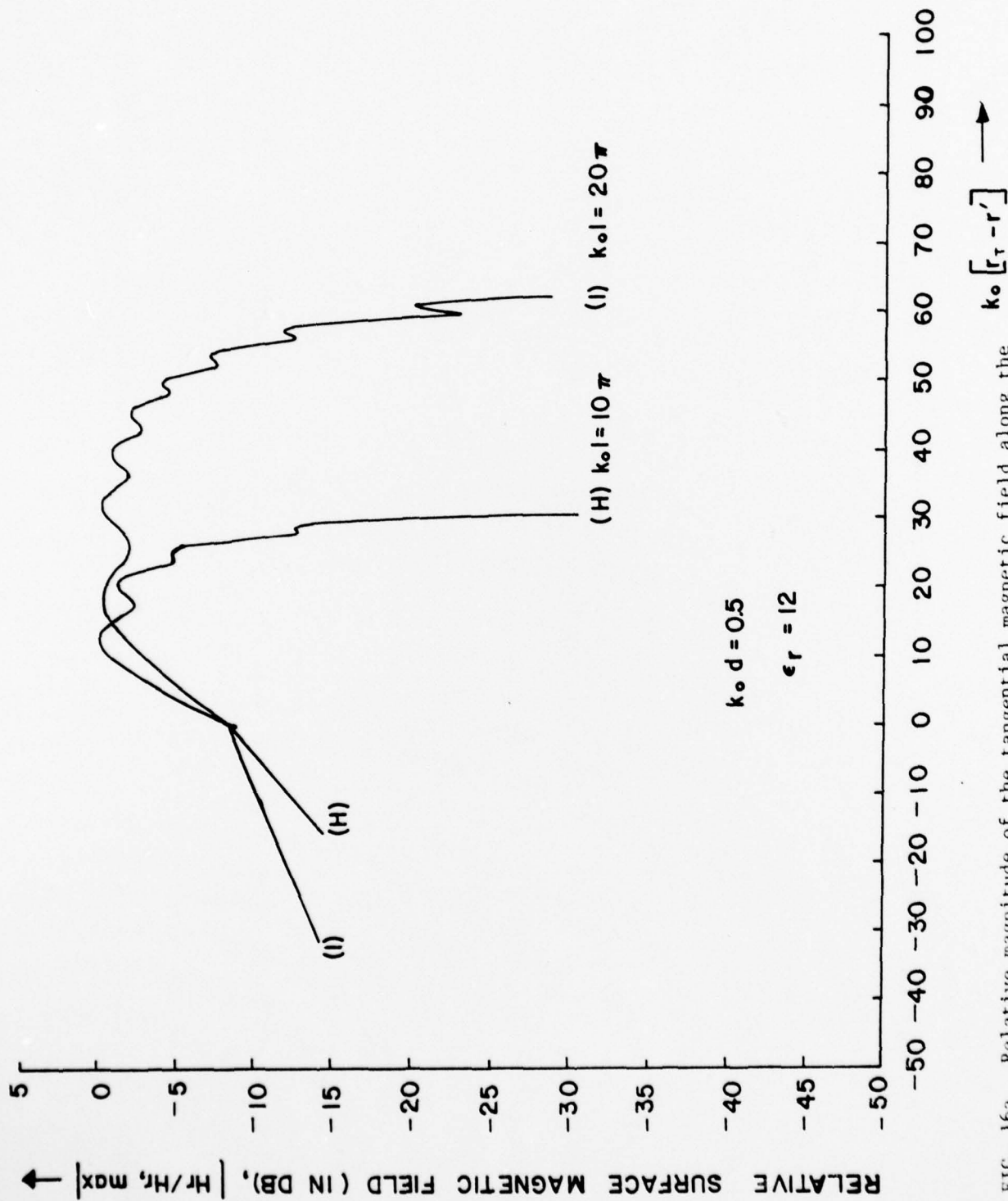
-59-

FIG. 14a. Relative magnitude of the tangential magnetic field along the wedge surface and along its geometric extension into the evanescent region of the slab.

FIG. 14b. Phase difference between the magnetic field H_r and a plane wave along the wedge surface and along its geometric extension into the evanescent region of the slab.

FIG. 15a. Relative magnitude of the tangential magnetic field along the wedge surface and along its geometric extension into the evanescent region of the slab.

$k_o l = 95.49$

$k_o d = 1.0$

RELATIVE SURFACE MAGNETIC FIELD (IN DB), $|H_\tau/H_{\tau,\,max}|$

$k_o [r_\tau - r']$ ⟶

(G) $\epsilon_r = 2.00$
(E) $\epsilon_r = 2.56$
(F) $\epsilon_r = 3.24$

FIG. 15b. Phase difference between the magnetic field H_r and a plane wave along the wedge surface and along its geometric extension into the evanescent region of the slab.
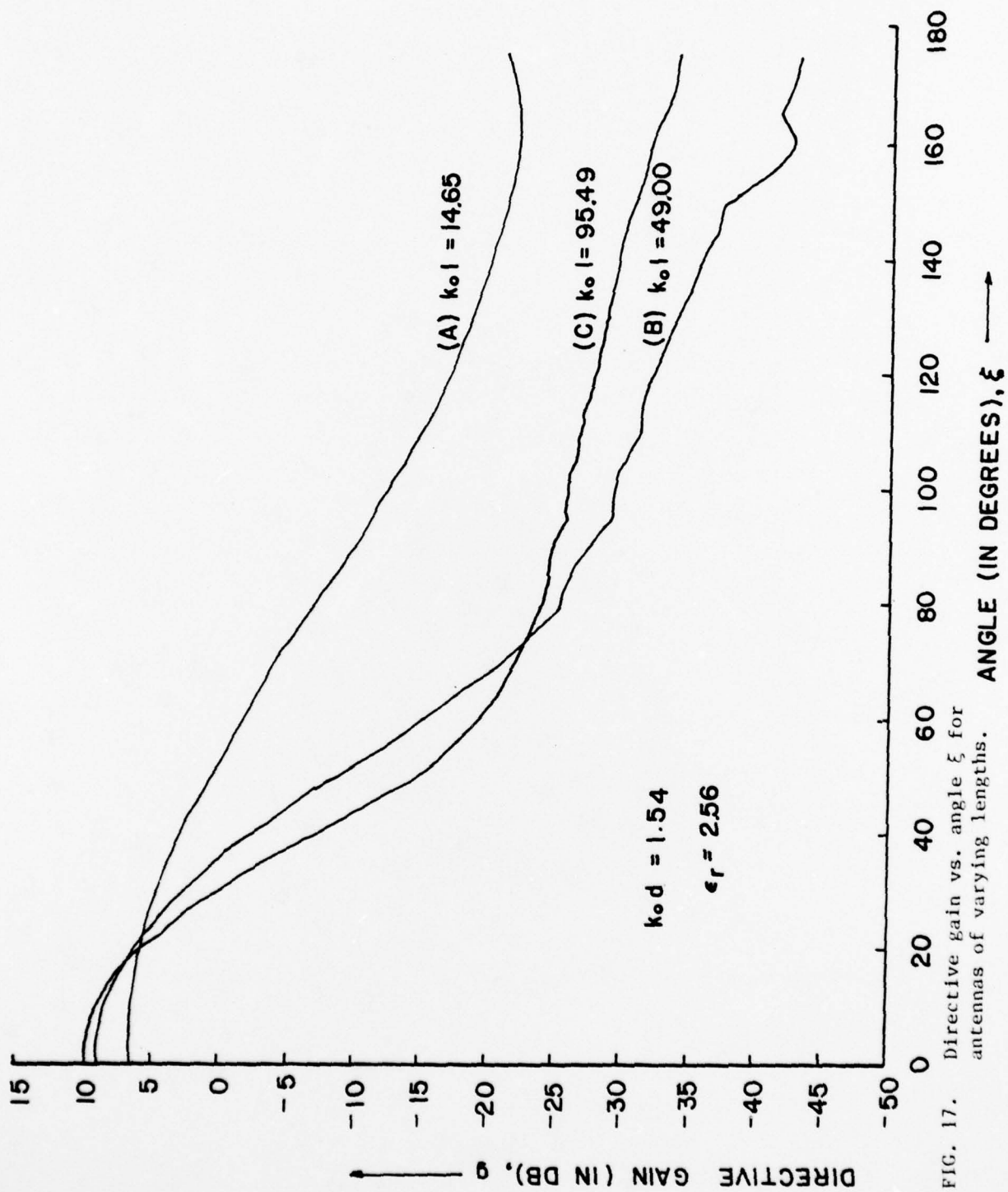
-63-

FIG. 16a. Relative magnitude of the tangential magnetic field along the wedge surface and along its geometric extension into the eva-nescent region of the slab.

-64-
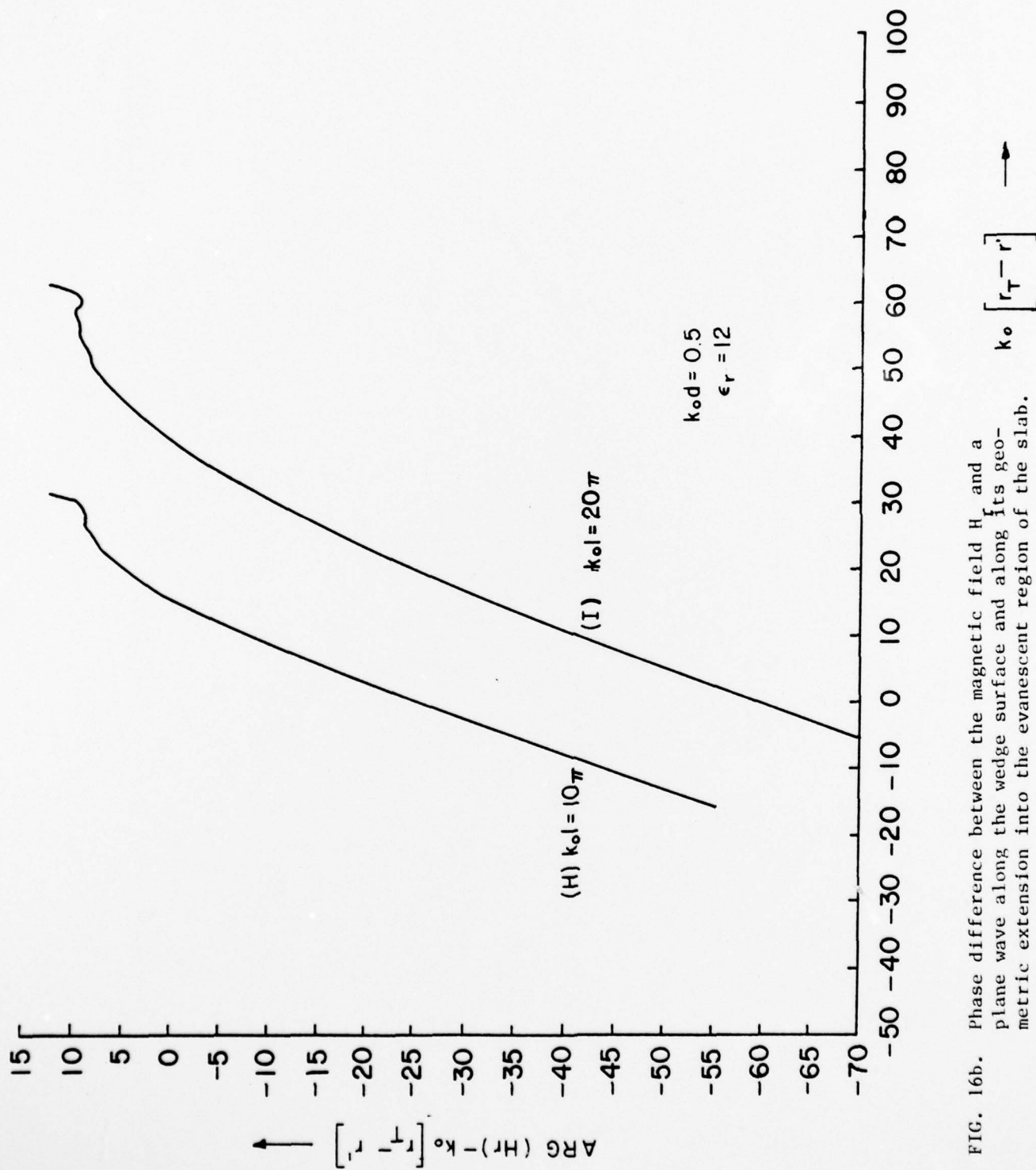
FIG. 16b. Phase difference between the magnetic field H_f and a plane wave along the wedge surface and along its geometric extension into the evanescent region of the slab.

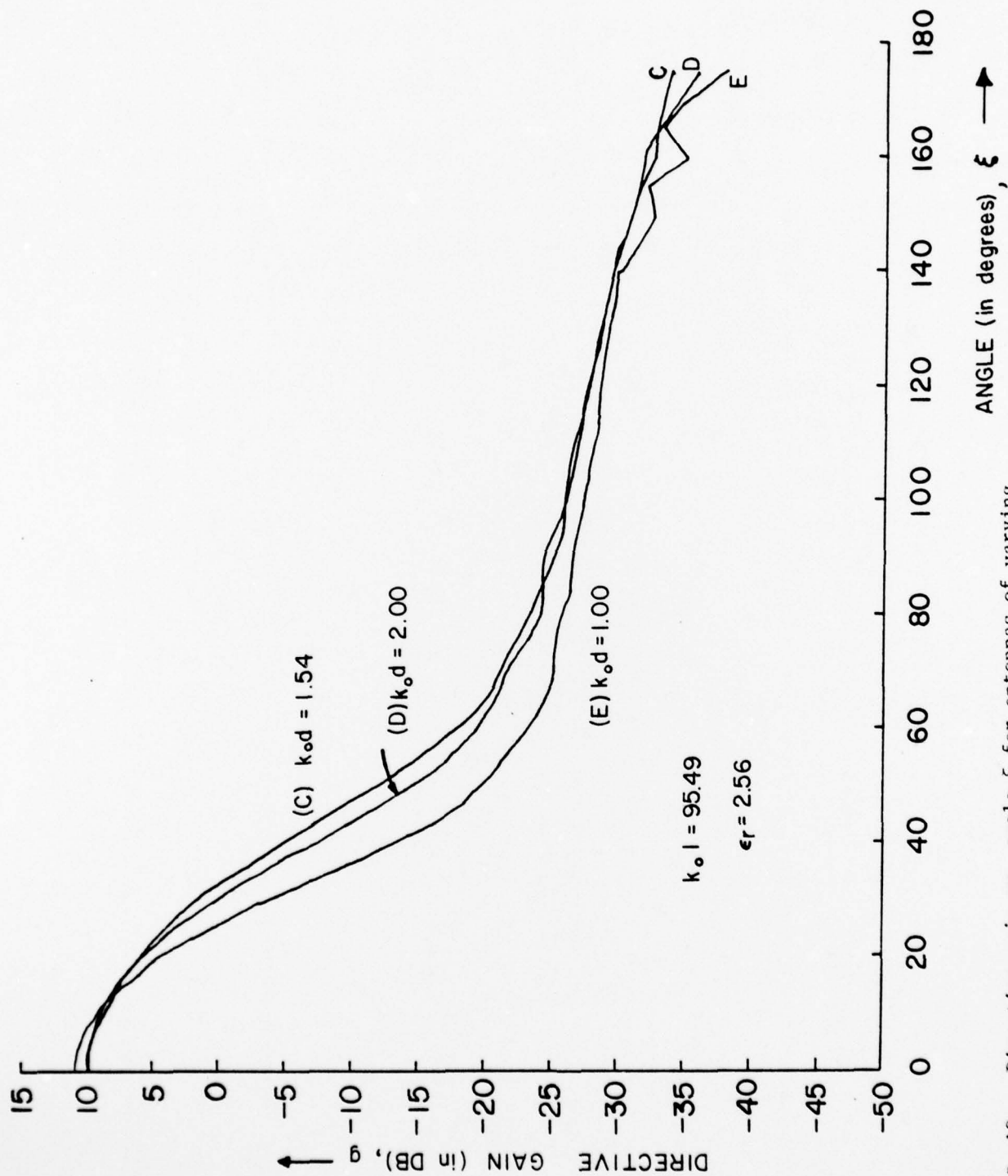FIG. 17. Directive gain vs. angle ξ for antennas of varying lengths.

$k_o d = 1.54$

$\epsilon_r = 2.56$

(A) $k_o l = 14.65$

(C) $k_o l = 95.49$

(B) $k_o l = 49.00$

ANGLE (IN DEGREES), ξ ⟶

DIRECTIVE GAIN (IN DB), g

-66-

FIG. 18.   Directive gain vs. angle ξ for antennas of varying
slab width.
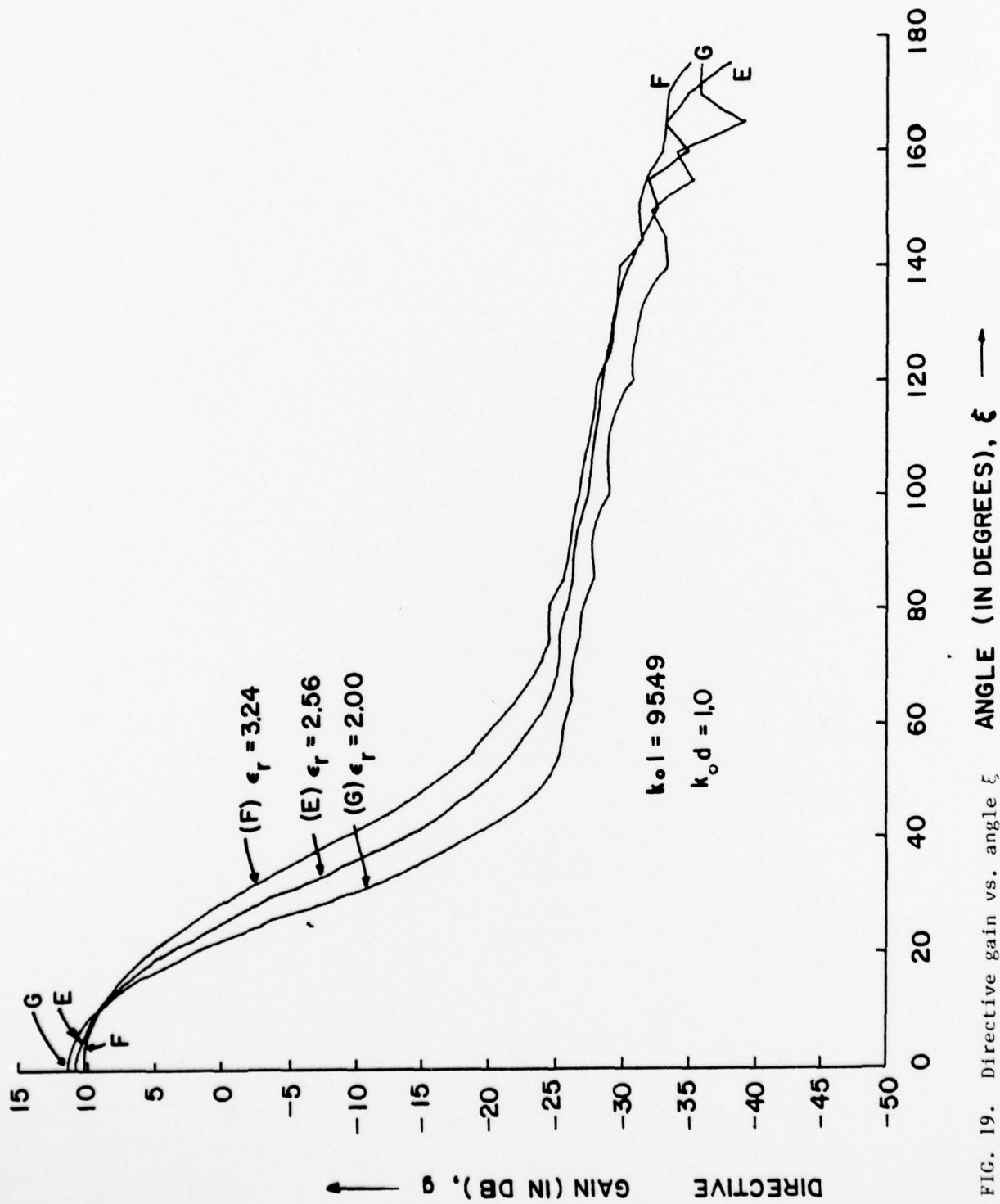
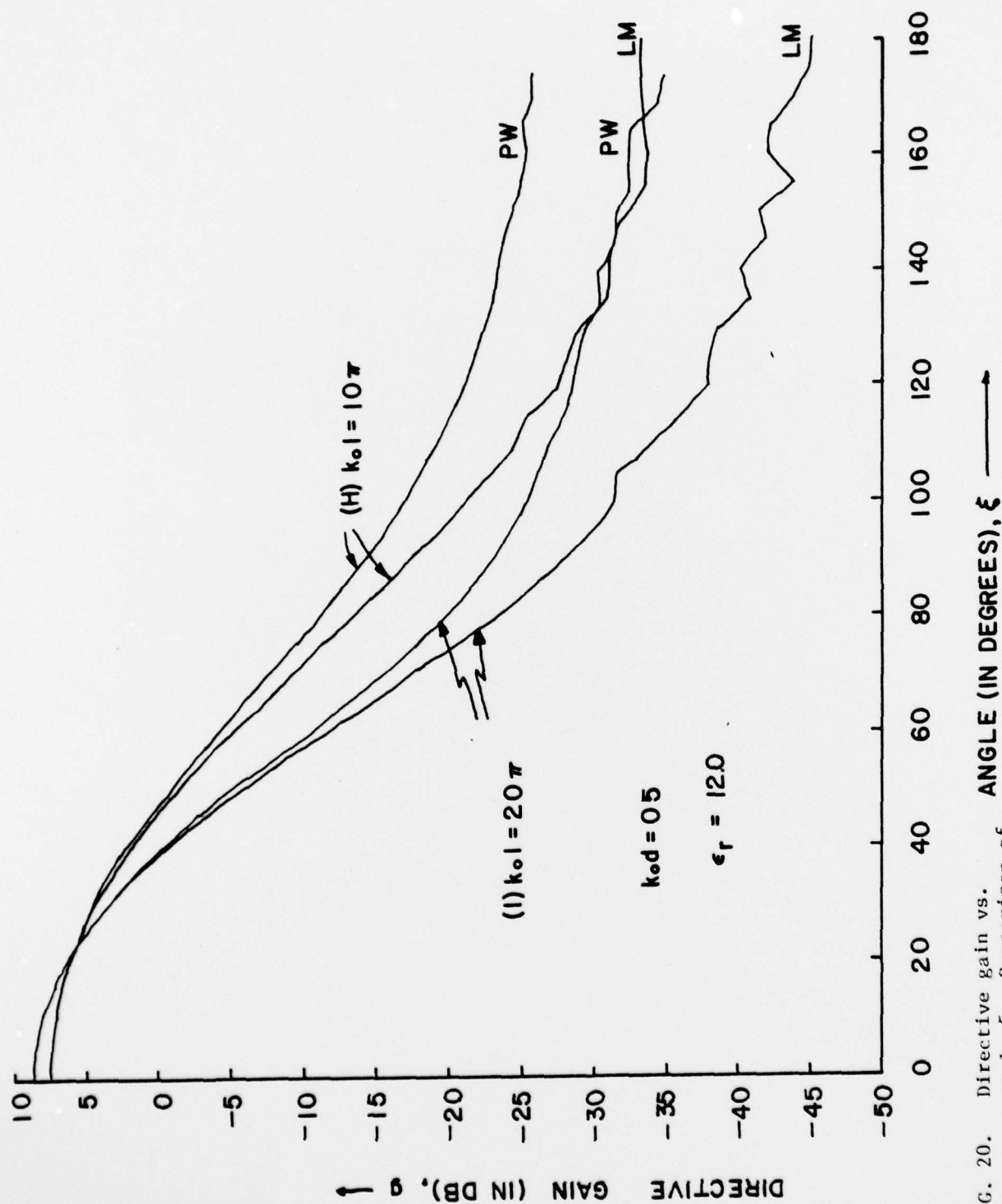FIG. 19. Directive gain vs. angle ξ for antennas of varying relative permittivity.

FIG. 20. Directive gain vs. angle ξ. Comparison of approaches: plane wave (PW) vs. local mode (LM).
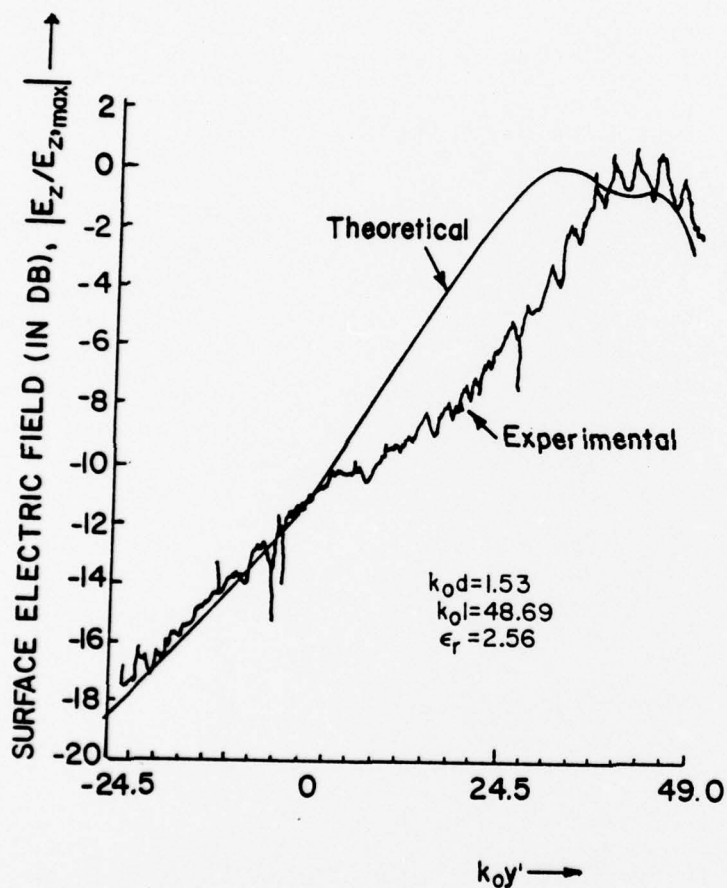
FIG. 21. Relative magnitude of the electric field along the wedge surface and along its geometric extension into the evanescent region of the slab - experimental vs. theoretical results.
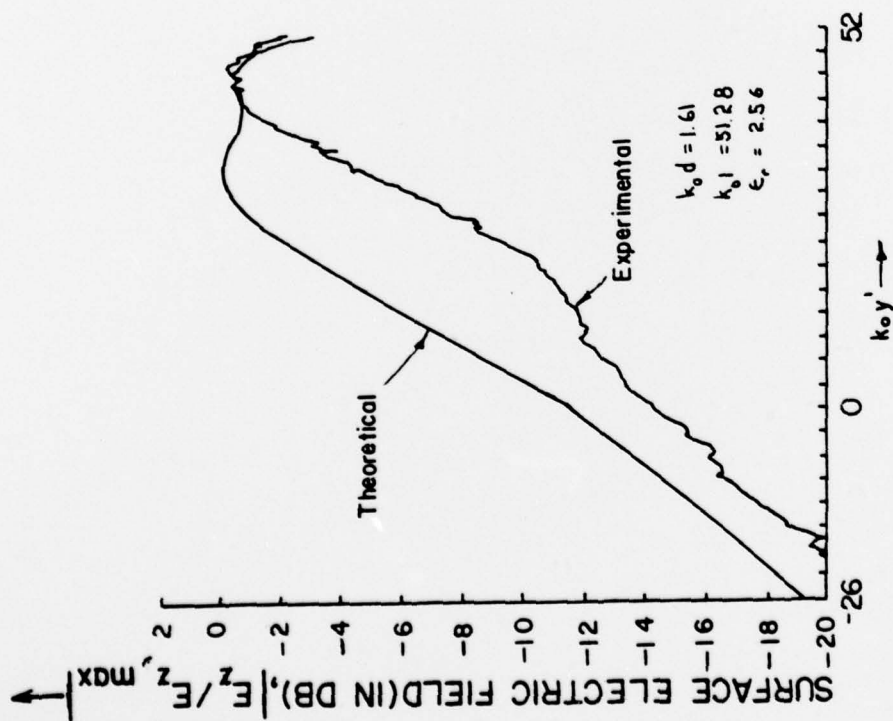
FIG. 22. Relative magnitude of the electric field along the wedge surface and along its geometrical extension into the evanescent region of the slab - experimental vs. theoretical results.
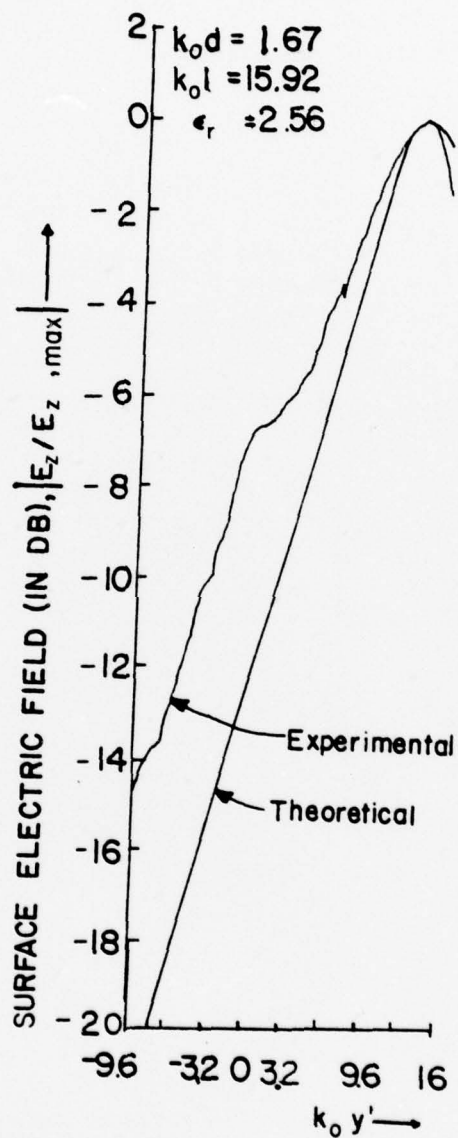
FIG. 23. Relative magnitude of the electric field along the wedge surface and along its geometric extension into the evanescent region of the slab - experimental vs. theoretical results.

-72-